# A discontinuous Galerkin residual-based variational multiscale method for modeling subgrid-scale behavior of the viscous Burgers equation

Stoter, Stein K.F.; Turteltaub, Sergio R.; Hulshoff, Steven J.; Schillinger, Dominik

**DOI**
10.1002/fld.4662

**Publication date**
2018

**Document Version**
Final published version

**Published in**
International Journal for Numerical Methods in Fluids

**Citation (APA)**
Stoter, S. K. F., Turteltaub, S. R., Hulshoff, S. J., & Schillinger, D. (2018). A discontinuous Galerkin residual-based variational multiscale method for modeling subgrid-scale behavior of the viscous Burgers equation. *International Journal for Numerical Methods in Fluids*, *88*(5), 217-238. https://doi.org/10.1002/fld.4662

Received: 23 October 2017 | Revised: 10 May 2018 | Accepted: 17 June 2018

DOI: 10.1002/fld.4662

RESEARCH ARTICLE

WILEY

# A discontinuous Galerkin residual-based variational multiscale method for modeling subgrid-scale behavior of the viscous Burgers equation

Stein K.F. Stoter[1,2] | Sergio R. Turteltaub[2] | Steven J. Hulshoff[2] | Dominik Schillinger[1]

[1]Department of Civil, Environmental, and Geo-Engineering, University of Minnesota, Minneapolis, Minnesota

[2]Faculty of Aerospace Engineering, Delft University of Technology, Delft, The Netherlands

**Correspondence**
Stein K.F. Stoter, Department of Civil, Environmental, and Geo-Engineering, University of Minnesota, Minneapolis, MN 55455.
Email: Stote031@umn.edu

**Funding information**
National Science Foundation, Grant/Award Number: 1651577

**Summary**

We initiate the study of the discontinuous Galerkin residual-based variational multiscale (DG-RVMS) method for incorporating subgrid-scale behavior into the finite element solution of hyperbolic problems. We use the one-dimensional viscous Burgers equation as a model problem, as its energy dissipation mechanism is analogous to that of turbulent flows. We first develop the DG-RVMS formulation for a general class of nonlinear hyperbolic problems with a diffusion term, based on the decomposition of the true solution into discontinuous coarse-scale and fine-scale components. In contrast to existing continuous variational multiscale methods, the DG-RVMS formulation leads to additional fine-scale element interface terms. For the Burgers equation, we devise suitable models for all fine-scale terms that do not use ad hoc devices such as eddy viscosities but instead directly follow from the nature of the fine-scale solution. In comparison to single-scale discontinuous Galerkin methods, the resulting DG-RVMS formulation significantly reduces the energy error of the Burgers solution, demonstrating its ability to incorporate subgrid-scale behavior in the discrete coarse-scale system.

**KEYWORDS**

Burgers turbulence, discontinuous Galerkin methods, residual-based multiscale modeling, variational multiscale method

## 1 | INTRODUCTION

The variational multiscale (VMS) method is a paradigm for incorporating the fine-scale effects of a partial differential equation (PDE) into the coarse-scale finite element solution by means of a multiscale model.[1-3] So far, the VMS method, particularly its residual-based format, has played an important role in designing efficient finite element discretization schemes for hyperbolic problems, including those described by Navier-Stokes equations. On the one hand, its ability to model subgrid-scale behavior has motivated the use of the VMS method as a large-eddy simulation (LES)–type turbulence model.[4-7] On the other hand, its intimate relation to stabilization mechanisms has enabled VMS-based derivations of stabilized finite element schemes.[8-10] Another important paradigm in the context of hyperbolic problems is the discontinuous Galerkin (DG) method.[11,12] The significant impact of DG methods in recent years has been based on a series of advantageous properties, such as its natural stability for advective operators, its local conservation properties, the potential

  

use of basis functions of arbitrary order on unstructured meshes, straightforward *hp*-adaptivity, and its suitability for parallel computing.[13-19]

Motivated by the individual success of the VMS and DG paradigms, we have developed a general form of the VMS method in a DG framework. In the past, there have been efforts to combine the two approaches, such as the multiscale DG methods introduced in the works of Bochev et al,[20] Buffa et al,[21] and Hughes et al[22] and methods for constructing discontinuous fine-scale bubble functions.[23,24] These methods, however, maintain a continuous solution space for the coarse-scale problem and use discontinuous representations of the fine scales only. They thus fundamentally differ from the original VMS idea, that is, the decomposition of the true solution into a discontinuous coarse-scale function space and an accompanying discontinuous fine-scale function space. While several authors have investigated the enhancement of DG methods with fine-scale eddy viscosity or wall models,[25-31] DG methods based on a residual-based VMS subgrid-scale model are still largely unexplored. To some extent, this may be attributed to the importance of coarse-scale continuity in the derivation of the VMS method.[2,10,32]

The discontinuous Galerkin residual-based variational multiscale (DG-RVMS) method that we have presented recently in a preliminary work[33] no longer relies on the level of continuity of the coarse-scale function space. On the basis of the decomposition of the true solution into discontinuous coarse-scale and fine-scale components, it features two types of fine-scale contributions. The first is a fine-scale volumetric term, which is formulated in terms of a residual-based model that also takes into account the nonhomogeneous fine-scale element boundary values. The second are independent fine-scale terms at element interfaces, which are formulated in terms of a new fine-scale "interface model." In a preliminary work,[33] we demonstrated for the one-dimensional Poisson problem that existing DG formulations, such as the symmetric interior penalty (IP) method,[14] can be rederived by choosing particular fine-scale interface models. The multiscale formulation thus opens the door for a new perspective on DG methods and their numerical properties. In our previous work,[33] this was demonstrated for the one-dimensional advection-diffusion problem, where the use of upwind numerical fluxes was shown to be interpretable as an ad hoc remedy for missing volumetric fine-scale terms.

In this paper, we begin the exploration of the DG-RVMS method as a framework for modeling subgrid-scale effects on the computational coarse-scale solution. Since this work represents our first step in this direction, we restrict ourselves to the transient nonlinear viscous Burgers equation in one space dimension. Such a model problem provides an initial indication of the quality of turbulence models for more complex fluid mechanics problems. This is based on the key observation that the energy dissipation in the solution of the one-dimensional Burgers equation follows an energy cascade that is analogous to the energy cascade observed in turbulent solutions of the Navier-Stokes equations in three dimensions.[34-36] In both systems, the kinetic energy is, on average, transported to higher-frequency modes by nonlinear hyperbolic terms in the PDE, where it is finally dissipated by the viscous term. Accurate reproduction of this scale interaction in the Burgers equation constitutes an initial representative test of the performance of the new DG-RVMS formulation and associated fine-scale models for representing subgrid-scale behavior.

This paper is organized as follows. In Section 2, we review the essential properties of the Burgers equation in view of its inherent energy cascade. In Section 3, we summarize the DG-RVMS formulation according to our preliminary work[33] and extend it to a general class of nonlinear hyperbolic PDEs. In Section 4, we specify the formulation for the one-dimensional Burgers equation, discretized by higher-order DG finite elements in space and a fourth-order Runge-Kutta method in time. In Section 5, we present numerical results that demonstrate the improved accuracy of the finite element solution, when subgrid scales are represented by fine-scale models in the context of the DG-RVMS formulation. In Section 6, we draw conclusions and discuss the potential of the DG-RVMS method for modeling subgrid-scale behavior in other contexts.

## 2 | THE BURGERS EQUATION AND ITS MULTISCALE SOLUTION BEHAVIOR

We define the following initial boundary value problem on a periodic one-dimensional domain $\Omega$, based on the forced viscous Burgers equation:

$$\begin{cases} u_t - \nu\Delta u + (u\cdot\nabla)u = g, & \text{in } \Omega\times(t^0,T] \\ u = u(t^0), & \text{on } \Omega\times\{t^0\}, \end{cases} \tag{1}$$

where $\nu$ is the viscosity coefficient and $g$ is the source function. The solution $u$, which can loosely be interpreted as the velocity, is propagated from its initial condition $u(t^0)$ at time $t = t^0$ until $t = T$.

## 2.1 | Decomposition into diffusion and transport equations

In fluid dynamics, interactions between scales are often characterized in terms of an energy transfer.[36,37] Similarly, the scale interaction in the solution of the Burgers equation (1) may be characterized by the energy distribution in the frequency domain. To this end, we define the energy of the Burgers solution to be analogous to the kinetic energy per unit mass of a fluid as

$$E = \frac{1}{2}u^2. \tag{2}$$

To understand the fine-scale behavior, we separately study the two types of equations found in (1), namely, the parabolic diffusion equation and the hyperbolic nonlinear transport equation, as follows:

$$u_t - \nu u_{xx} = 0 \tag{3}$$

$$u_t + u\,u_x = u_t + \frac{1}{2}(u^2)_x = 0. \tag{4}$$

The nonlinear transport equation (4) is often referred to as the inviscid Burgers equation. When we assume a sufficiently smooth solution $u$ on a one-dimensional periodic domain, both (3) and (4) conserve the total quantity $u$. This can be shown as follows:

$$\begin{aligned}
\int_{x_0}^{x_1} (u_t - \nu u_{xx})\mathrm{d}x &= \frac{\mathrm{d}}{\mathrm{d}t}\int_{x_0}^{x_1} u\,\mathrm{d}x + \nu u_x\Big|_{x_0} - \nu u_x\Big|_{x_1} = 0 \\
\int_{x_0}^{x_1} \left(u_t + \frac{1}{2}(u^2)_x\right)\mathrm{d}x &= \frac{\mathrm{d}}{\mathrm{d}t}\int_{x_0}^{x_1} u\,\mathrm{d}x - \frac{1}{2}u^2\Big|_{x_0} + \frac{1}{2}u^2\Big|_{x_1} = 0.
\end{aligned} \tag{5}$$

When $x_0$ and $x_1$ are the end points of the periodic domain $\Omega$, it holds for both equations that

$$\frac{\mathrm{d}}{\mathrm{d}t}\int_{\Omega} u\ \mathrm{d}x = 0. \tag{6}$$

## 2.2 | Evolution of energy spectra in the diffusion and transport equations

Despite the conservation of $u$ in both PDEs, the corresponding solutions exhibit very different energy spectra. We illustrate the evolution of these energy spectra using analytically constructed examples. To obtain the energy spectrum of a solution, we make use of the discrete Fourier transform (DFT) with $N$ sampling points. The spectral energy associated with wave number $k$ is defined as

$$E(k) = \begin{cases} \frac{\pi}{N^2}\,|\mathrm{DFT}(k)|^2, & \text{when } k = 0 \\ \frac{2\pi}{N^2}\,|\mathrm{DFT}(k)|^2, & \text{when } k > 0. \end{cases} \tag{7}$$

Making use of Parseval's identity, we can observe that, as $N \to \infty$, the sum of spectral energies is equal to the total solution energy in one period of the domain, which is normalized to have a width of $2\pi$, as follows:

$$E_{\mathrm{tot}} = \frac{1}{2}\int_0^{2\pi} u(x)^2\mathrm{d}x \approx \frac{\pi}{N}\sum_{\hat{x}=0}^{N-1} u\Big(\frac{2\pi}{N^2}\hat{x}\Big)^2 = \frac{\pi}{N^2}\sum_{n=-\lfloor N/2\rfloor}^{\lfloor N/2\rfloor} |\mathrm{DFT}(n)|^2 = \sum_{k=0}^{\lfloor N/2\rfloor} E(k). \tag{8}$$

We consider a periodic domain of width $2\pi$. As an initial condition, we use a repeated Weibull distribution, given by (9), with shape parameter $\alpha = 2.5$ and scale parameter $\beta = 2.5$. The initial condition is propagated until $t = 4.5$.

$$u(x) = \frac{\alpha}{\beta^\alpha} x_0^{\alpha-1} e^{-(x_0/\beta)^\alpha} \quad \text{where } x_0 = x \bmod 2\pi \tag{9}$$

For the diffusion equation, we use Fourier analysis to obtain the solution at different time instants. Figure 1A illustrates the evolution of the solution for a viscosity coefficient $\nu = 0.3$. Figure 1B plots the energy spectra, according to (7), that correspond to the plotted solutions at different time instants. We observe that both the solutions and the associated energy spectra show a rapid damping of high-frequency modes, emphasizing coarse-scale solution components.

For the nonlinear transport equation, we use the method of characteristics to advance the solution in time. Figure 2A illustrates the evolution of the solution in time for the given initial condition. We observe that a shock wave is formed

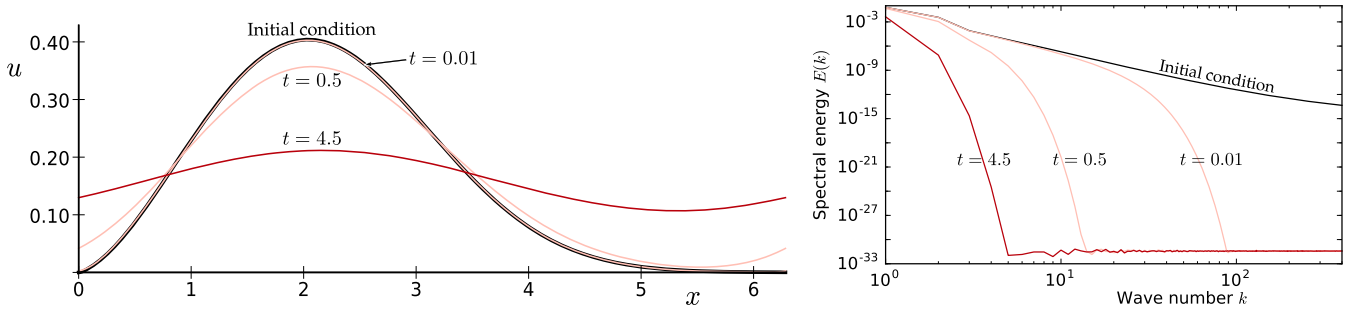


**(A)** Spatial solutions. **(B)** Energy spectra.

**FIGURE 1** Solution of the diffusion equation at different time instants. A, Spatial solutions; B, Energy spectra [Colour figure can be viewed at wileyonlinelibrary.com]

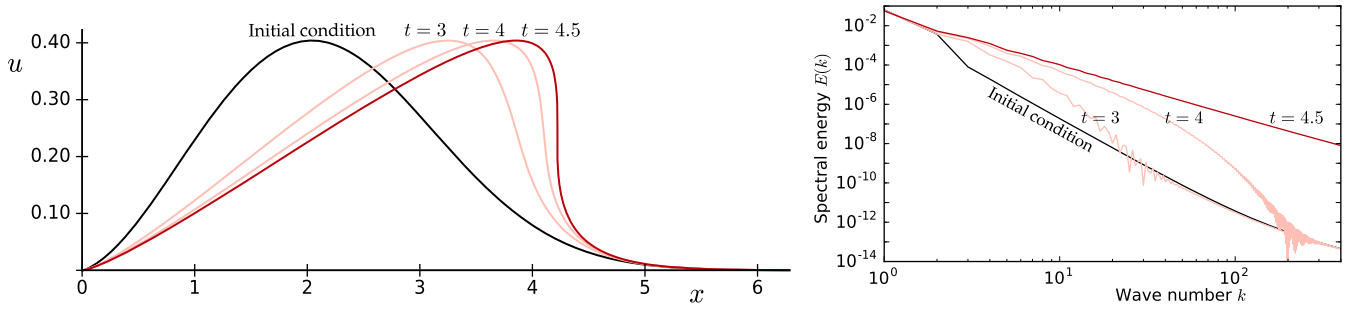


**(A)** Spatial solutions. **(B)** Energy spectra.

**FIGURE 2** Solution of the nonlinear transport equation at different time instants. A, Spatial solutions; B, Energy spectra [Colour figure can be viewed at wileyonlinelibrary.com]

at the final time instant $t = 4.5$. Figure 2B plots the energy spectra that correspond to the displayed solution fields at different times. We observe that in contrast to the diffusion equation, the nonlinear transport equation transfers energy toward the higher frequencies. The sharp gradient at the shock front requires a wide distribution of energy components in the frequency domain, emphasizing fine-scale solution components.

## 2.3 | Balance of energy spectra and Burgers turbulence

When the diffusion equation (3) and the transport equation (4) are combined to form the Burgers equation (1), the solution must represent a balance between the two conflicting energy evolutions. We illustrate the balance in the energy spectrum evolution with a numerical example described in the work of Hulshoff.[38] We consider (1) on a periodic domain of width $2\pi$ with viscosity coefficient $\nu = 2\pi/1000$, constant initial condition $u(t^0) = 1$, and source function $g(x,t) = 0.1\sin(x-t)$ that is periodic in space and time. This problem was investigated in the work of Hulshoff.[38] We discretize the domain with 8192 linear finite elements in space and use the fifth-order accurate explicit Dormand-Prince Runge-Kutta method in time with a time-step size of $\Delta t = 3.2\cdot 10^{-5}$. The spatial mesh resolution is thereby equal to that of the direct numerical simulation (DNS) described in the work of Hulshoff,[38] whereas we use a smaller time step and a time integration method of higher order. Figure 3A,B plots solutions and the corresponding energy spectra at different time instants. We observe that periodic forcing creates a wave that travels to the right through the periodic domain. From $t = 6\pi$ onward, the shape of the wave that is translated through the periodic domain remains practically unchanged, so that the corresponding energy spectrum is steady.

The steady energy spectrum shown in Figure 3B illustrates the characteristic multiscale solution behavior of the Burgers equation. The nonlinear hyperbolic nature of the equation results in a solution that approaches a shock wave. In the frequency response, this corresponds to energy being transferred to the high-frequency modes. At the high-frequency range, the energy is dissipated by the viscous term of the equation. We note that the noisy behavior past $k = 10^3$ is the result of the limited machine accuracy, where $E(k) \approx 10^{-32}$ roughly corresponds to the square of the double-precision machine epsilon.

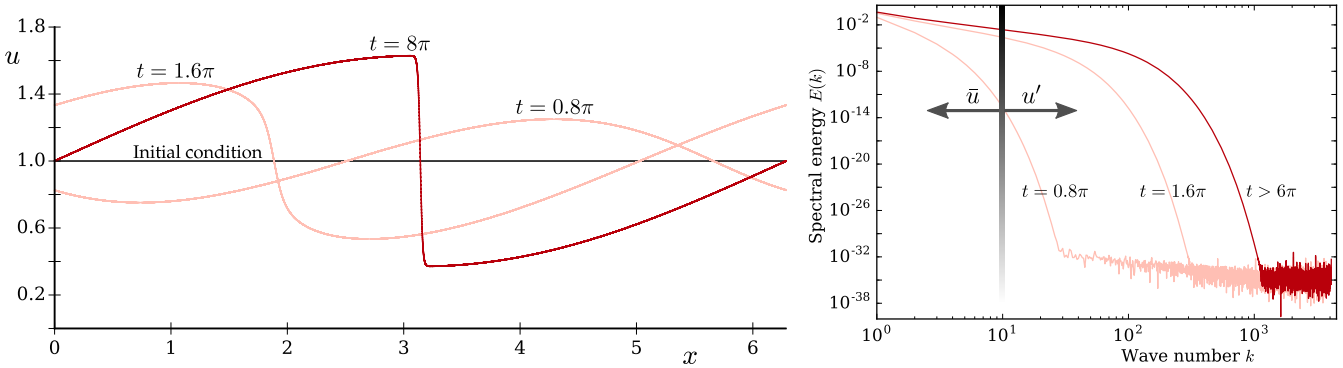


**(A)** Spatial solutions. **(B)** Energy spectra.

**FIGURE 3** Direct numerical simulation solution of the Burgers problem at different time instants. A, Spatial solutions; B, Energy spectra [Colour figure can be viewed at wileyonlinelibrary.com]

As we use a sufficiently fine discretization in space and time, all scales of the Burgers solution can be resolved with sufficient accuracy. In practical applications, however, such DNS discretization is prohibitively expensive, so that coarser discretizations must be used that can only represent the coarse-scale behavior of the PDE. As conceptually illustrated in Figure 3B, the coarse-scale finite element solution (denoted by $\bar{u}$) covers only the low-frequency modes. In this situation, a subgrid-scale model, for example, VMS based, that reproduces the effect of the scale interaction with fine-scale solution components (denoted by $u'$) is essential for an accurate coarse-scale solution. Without a suitable subgrid-scale model, the coarse-scale solution will tend to overemphasize certain energy components, since they cannot be dissipated at the fine scales.[38] In the following sections, we will develop a residual-based fine-scale model that can be used in a DG VMS formulation of the Burgers equation.

## 3 | VMS FORMULATION IN A DISCONTINUOUS APPROXIMATION SPACE

In this section, we extend the DG-RVMS method, introduced in our preliminary work,[33] to nonlinear hyperbolic problems with a viscous term. For a periodic domain $\Omega$, this class of boundary value problems is defined as

$$\begin{cases} u_t - \nu\Delta u + \nabla \cdot f(u) = g(x,t), & \text{in } \Omega \times (t^0, T] \\ u = u(t^0), & \text{on } \Omega \times \{t^0\}, \end{cases} \tag{10}$$

where $f(u)$ is a (potentially nonlinear) flux function. We assume that the diffusion coefficient is sufficiently large to ensure that the true solution is at least $C^1$-continuous in space and time. We emphasize that the class of problems described by (10) contains the Burgers model problem (1) as a special case.

### 3.1 | Space-time VMS formulation

Following the VMS procedure described in the work of Bazilevs et al,[5] we divide the temporal domain into $N$ time slabs of domain $(t^n, t^{n+1})$, where $n = 0, \ldots, N-1$. A separate initial boundary value problem can be posed for each time slab. The initial value within a time slab is the final value of the previous time slab. For discretizing the space-time domain, we consider the following function space:

$$\mathcal{V}^n(h) = \left\{ v \in L^2\left(\Omega \times [t^n, t^{n+1}]\right) : v\big|_Q \in C^0 \forall Q \in \mathcal{T}_Q,\ v = h \text{ on } \Omega \times \{t^n\} \right\}, \tag{11}$$

where $Q$ is a space-time element in the set of space-time elements $\mathcal{T}_Q = \{Q\}$ that spans the time slab. Figure 4 illustrates the space-time domain and its discretization for the case of a one-dimensional spatial domain. Each space-time element is constructed as a spatial element $K$ advanced in time: $Q = K \times (t^n, t^{n+1})$. For completeness, we also define a computational mesh $\mathcal{T} = \{K\}$, which is the set of spatial elements. We emphasize that (11) allows trial and test functions that are discontinuous from element to element.

We derive the weak formulation of problem (10) on each time slab by the method of weighted residuals that we individually apply to each space-time element. This ensures that the derivatives remain well defined within the respective

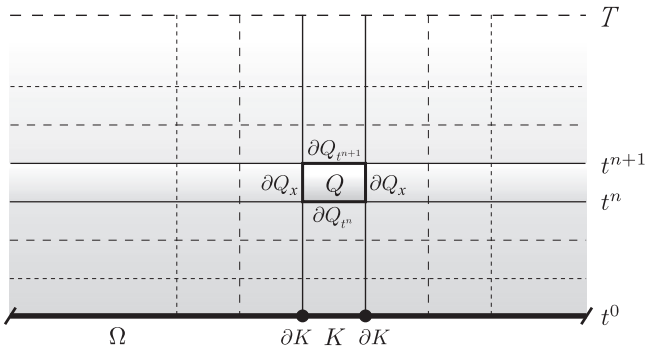


**FIGURE 4** Definition of the domain and discretization

element domain. Additionally, we impose transmission conditions that act on the element interfaces to couple the elements and to ensure the uniqueness of the solution. Making use of the definitions summarized in Table 1, the weak formulation reads as follows:

$$\text{Find}\, u \in \mathcal{V}^n\left(u(t^n)\right) \text{ s.t.:} \quad \begin{cases} \sum\limits_{Q\in\mathcal{T}_Q} (w, u_t - \nu\Delta u + \nabla\cdot f(u))_Q = \sum\limits_{Q\in\mathcal{T}_Q} (w,g)_Q & \forall w \in \mathcal{V}^n(0) \\ [\![u]\!] = 0, & \text{on } \partial Q_x \quad \forall Q \in \mathcal{T}_Q \\ [\![\nabla u]\!] = 0, & \text{on } \partial Q_x \quad \forall Q \in \mathcal{T}_Q. \end{cases} \tag{12}$$

In the next step, we introduce the split of the true solution $u$ into a coarse-scale solution $\bar{u}$ and a complementary fine-scale solution $u'$. First, we define a subspace of $\mathcal{V}^n$ that represents the coarse-scale function space. This will be the finite-dimensional discontinuous approximation space $\overline{\mathcal{V}}^n$, ie,

$$\overline{\mathcal{V}}^n(\mathrm{g}) = \left\{ v \in L^2\left(\Omega\times[t^n,t^{n+1}]\right) \,:\, v\Big|_K \in P^p(Q)\,\forall Q\in\mathcal{T}_Q,\, v = g \text{ at } t = t^n \right\}. \tag{13}$$

Next, the coarse-scale solution is defined as the component of $u$ that can be precisely represented in the coarse-scale function space. A projector $\mathcal{P} : \mathcal{V}^n \to \bar{\mathcal{V}}^n$ is required to obtain $\bar{u}$ as a projection of $u$ onto $\bar{\mathcal{V}}^n$, ie,

$$\bar{u} \equiv \mathcal{P}u \in \bar{\mathcal{V}}^n(\cdot). \tag{14}$$

The fine-scale solution $u'$ is thereby naturally defined as the difference between the true solution $u$ and the coarse-scale solution $\bar{u}$, ie,

$$u' \equiv u - \bar{u} \;\Rightarrow\; u = \bar{u} + u'. \tag{15}$$

**TABLE 1** Collection of domain definitions

| | | |
|---|---|---|
| Jump operator | $[\![w]\!]$ | $= w^+\cdot n^+ + w^-\cdot n^-$ |
| Average operator | $\{\!\{w\}\!\}$ | $= \frac{1}{2}(w^+ + w^-)$ |
| Volume $L^2$-inner product | $(w,u)_K$ | $= \int_K w\cdot u$ |
| Surface $L^2$-inner product | $\langle w\cdot n, u\rangle_{\partial K}$ | $= \int_{\partial K} w\cdot n u$ |
| Space domain | $\Omega$ | (Periodic) |
| Element space domain | $K$ | (With boundary $\partial K$) |
| Space-time element | $Q$ | $= K\times(t^n, t^{n+1})$ |
| Temporal boundary of $Q$ | $\partial Q_{t^n}$ | $= K\times\{t^n\}$ |
| Spatial boundary of $Q$ | $\partial Q_x$ | $= \partial K\times(t^n, t^{n+1})$ |
| Numerical space domain | $\Omega_K$ | $= \bigcup\limits_{K\in\mathcal{T}} K$ s.t. $(w,u)_{\Omega_K} = \sum\limits_{K\in\mathcal{T}} (w,u)_K$ |
| Numerical space-time domain | $\Omega_Q$ | $= \bigcup\limits_{Q\in\mathcal{T}_Q} Q$ s.t. $(w,u)_{\Omega_Q} = \sum\limits_{Q\in\mathcal{T}_Q} (w,u)_Q$ |
| Element interfaces | $\Gamma$ | $= \bigcup\limits_{K\in\mathcal{T}} \partial K$ s.t. $\langle 1, [\![u]\!]\rangle_\Gamma = \sum\limits_{K\in\mathcal{T}} \langle 1, u\cdot n\rangle_{\partial K}$ |

According to this definition, the fine-scale solution and the discretization error are equivalent. Thereby, the design of subgrid-scale models and the design of the finite element scheme are unified. In contrast, for typical LES, the coarse-scale solution is defined by means of some filtering operator. Then, the development of a model that accurately captures the fine-scale effects and the task of numerically resolving the coarse-scale solution are two separate objectives.

When projector $\mathcal{P}$ is a linear, idempotent, surjective mapping, then the fine-scale solution is a member of the fine-scale space $\mathcal{V}'^n$. This is shown as follows:

$$\mathcal{P}u' = \mathcal{P}(u-\bar{u}) = \mathcal{P}u - \mathcal{P}(\mathcal{P}u) = 0 \;\Rightarrow\; u' \in \ker(\mathcal{P}) \equiv \mathcal{V}'^n(\cdot). \tag{16}$$

By construction of the fine-scale function space $\mathcal{V}'^n$, the coarse-scale and fine-scale function spaces form a direct sum decomposition of the space $\mathcal{V}^n$, as follows:

$$\mathcal{V}^n = \overline{\mathcal{V}}^n \oplus \mathcal{V}'^n. \tag{17}$$

By definition of the direct sum decomposition (17), any possible true solution $u \in \mathcal{V}^n$ maps *uniquely* to a coarse-scale solution $\bar{u} \in \overline{\mathcal{V}}^n$ and a fine-scale solution $u' \in \mathcal{V}'^n$. This ensures the well-posedness of the VMS formulation. By substituting the split (15) into the weak formulation (12), we obtain the following VMS formulation:

$$\begin{aligned}
&\text{Find } \bar{u}, u' \in \overline{\mathcal{V}}^n\left(\bar{u}(t^n)\right) \times \mathcal{V}'^n\left(u'(t^n)\right) \text{ s.t.:}\\
&\begin{cases}
\left(\bar{w}, \bar{u}_t + u'_t\right)_{\Omega_Q} - \left(\nu\bar{w}, \Delta\bar{u} + \Delta u'\right)_{\Omega_Q} + \left(\bar{w}, \nabla\cdot f(\bar{u}+u')\right)_{\Omega_Q} = (\bar{w}, g)_{\Omega_Q} & \forall \bar{w} \in \bar{\mathcal{V}}^n(0)\\
\left(w', \bar{u}_t + u'_t\right)_{\Omega_Q} - (\nu w', \Delta\bar{u} + \Delta u')_{\Omega_Q} + \left(w', \nabla\cdot f(\bar{u}+u')\right)_{\Omega_Q} = (w', g)_{\Omega_Q} & \forall w' \in \mathcal{V}^n(0)\\
[\![\bar{u}]\!] = -[\![u']\!], \quad \text{on } \partial Q_x & \forall Q \in \mathcal{T}_Q\\
[\![\nabla\bar{u}]\!] = -[\![\nabla u']\!], \quad \text{on } \partial Q_x & \forall Q \in \mathcal{T}_Q.
\end{cases}
\end{aligned} \tag{18}$$

In the next step, we will transfer the first line in (18), which we refer to as the coarse-scale weak formulation, into a discrete DG format. To this end, we first perform element-wise integration by parts on the different terms to find the following weak formulation:

$$\begin{aligned}
&\text{Find } \bar{u} \in \overline{\mathcal{V}}^n\left(\bar{u}(t^n)\right) \text{ s.t.:}\\
&(\bar{w}, \bar{u}_t)_{\Omega_Q} - (\bar{w}_t, u')_{\Omega_Q} + \sum_{Q\in\mathcal{T}_Q} -\langle\bar{w}, u'\rangle_{\partial Q_{t^n}} + \langle\bar{w}, u'\rangle_{\partial Q_{t^{n+1}}}\\
&\quad + (\nu\nabla\bar{w}, \nabla\bar{u})_{\Omega_Q} - \sum_{Q\in\mathcal{T}_Q}\langle\nu\bar{w}, \nabla\bar{u}\cdot n\rangle_{\partial Q_x} - (\nu\Delta\bar{w}, u')_{\Omega_Q} + \sum_{K\in\mathcal{T}}\left[\langle\nu\nabla\bar{w}\cdot n, u'\rangle_{\partial Q_x} - \langle\nu\bar{w}, \nabla u'\cdot n\rangle_{\partial Q_x}\right]\\
&\quad - \left(\nabla\cdot\bar{w}, f(\bar{u}+u')\right)_{\Omega_Q} + \sum_{Q\in\mathcal{T}_Q}\left\langle\bar{w}, f(\bar{u}+u')\cdot n\right\rangle_{\partial Q_x} = (\bar{w}, g)_{\Omega_Q} \qquad \forall\bar{w} \in \bar{\mathcal{V}}^n(0).
\end{aligned} \tag{19}$$

We would like to emphasize two points with regard to the weak form of (19). Firstly, it does not yet represent a unique scale decomposition. The projector that defines this scale decomposition manifests itself in (19) through the fine-scale terms. When we substitute the fine-scale contributions that precisely correspond to projector $\mathcal{P}$ from (16), only then do we obtain the coarse-scale solution $\bar{u}$ corresponding to (14). In practice, however, the exact form of these fine-scale terms is unknown. Secondly, the element-local derivation leads to basis functions that are completely decoupled from element to element. Some form of element coupling needs to be incorporated into the weak form in order to retrieve a global (solvable) system of equations.

Both of these points may be addressed by replacing the fine-scale terms with suitable models. Equation (19) includes two types of fine-scale terms that represent the complete scale interaction between the fine-scale and coarse-scale solutions. They can be classified as fine-scale volumetric terms that have been examined in classical continuous VMS formulations and fine-scale interface terms that originate from the lack of continuity of the coarse-scale basis. We consider these two types of fine-scale occurrences separately in the following two sections.

## 3.2 | General form of the fine-scale interface model

In (12), the weak form is defined on each element separately, whereas transmission conditions are included to couple the elements. These conditions must be incorporated into (19) to obtain a global system of equations. To do so, we make use

of the following identities that follow from the definition of the jump and average operators (see Table 1):

$$\begin{aligned} u'^{\pm} n^{\pm} &= \{\!\{ u' \}\!\} n^{\pm} + \frac{1}{2} [\![ u' ]\!] \\ \nabla u'^{\pm} \cdot n^{\pm} &= \{\!\{ \nabla u' \}\!\} \cdot n^{\pm} + \frac{1}{2} [\![ \nabla u' ]\!], \end{aligned} \tag{20}$$

where the fine-scale solution on either side of an element boundary is written as $u'^{+}$ or $u'^{-}$.

At this stage, we incorporate the multiscale-type transmission conditions from (18). The jump of the fine-scale solution is equal and opposite to the jump of the coarse-scale solution, thereby yielding

$$\begin{aligned} u'^{\pm} n^{\pm} &= \{\!\{ u' \}\!\} n^{\pm} - \frac{1}{2} [\![ \bar{u} ]\!] \\ \nabla u'^{\pm} \cdot n^{\pm} &= \{\!\{ \nabla u' \}\!\} \cdot n^{\pm} - \frac{1}{2} [\![ \nabla \bar{u} ]\!]. \end{aligned} \tag{21}$$

To eliminate all the fine-scale interface dependencies in (19), we write the remaining fine-scale terms as functions of coarse-scale interface terms, ie,

$$\begin{aligned} u'^{\pm} n^{\pm} &= \Phi n^{\pm} - \frac{1}{2} [\![ \bar{u} ]\!] \\ \nabla u'^{\pm} \cdot n^{\pm} &= \Theta \cdot n^{\pm} - \frac{1}{2} [\![ \nabla \bar{u} ]\!], \end{aligned} \tag{22}$$

where we introduce fine-scale interface models of the form

$$\begin{aligned} \{\!\{ u' \}\!\} &= \Phi(\{\!\{ \bar{u} \}\!\}, [\![ \bar{u} ]\!], \{\!\{ \nabla \bar{u} \}\!\}, [\![ \nabla \bar{u} ]\!], \dots) \\ \{\!\{ \nabla u' \}\!\} &= \Theta(\{\!\{ \bar{u} \}\!\}, [\![ \bar{u} ]\!], \{\!\{ \nabla \bar{u} \}\!\}, [\![ \nabla \bar{u} ]\!], \dots). \end{aligned} \tag{23}$$

By substituting (22) into the element boundary terms in (19), we obtain a global formulation where all elements are coupled. The choice of the fine-scale interface model and the associated assumptions should directly reflect the physics of the fine-scale behavior of the specific PDE at hand. In the next section, we will illustrate this for the example of the Burgers equation. Together with the fine-scale volumetric model, the choice of the fine-scale interface model determines the projector (14) that defines the split (15) into a coarse-scale solution and a fine-scale solution.

### 3.3 | General form of the fine-scale volumetric model

Classical VMS formulations that treat the fine-scale volumetric term with a residual-based model assume that the fine-scale solution vanishes on element interfaces.[2,5] In a DG setting, the fine-scale solution at element interfaces is generally nonzero, which follows directly from (21). When the coarse-scale DG solution exhibits large jumps across element interfaces, the fine-scale solution must have large values as well, thus having a significant impact on the fine-scale volumetric term in (19). To accommodate the presence of nonhomogeneous fine-scale solution values at element boundaries, we propose the following modifications to the classical residual-based volumetric fine-scale model.

We start by considering the fine-scale weak formulation in (18), where we may treat each space-time element separately, since all functions are discontinuous from element to element. On a space-time element $Q$, we rewrite the fine-scale weak formulation in such a way that each term on the left-hand side contains fine-scale components. Assuming that the fine-scale solution $u'$ typically represents a small perturbation with respect to the coarse-scale solution $\bar{u}$, we expand the flux function $f$ into a first-order Taylor approximation that is linear with respect to $u'$, ie,

$$f(\bar{u} + u') = f(\bar{u}) + \frac{\mathrm{d}f}{\mathrm{d}u}(\bar{u}) u' + \mathcal{O}(u'^2). \tag{24}$$

Even though the numerical experiments show that this assumption is often violated, the resulting model approximation proves effective. We substitute this approximation into the fine-scale weak formulation and obtain

$$\begin{aligned} \text{Find } \tilde{u}' \in \mathcal{V}'^n\left(u'(t^n)\right) \text{ s.t.: } & \left(w', \tilde{u}'_t\right)_Q - \left(\nu w', \Delta \tilde{u}'\right)_Q + \left(w', \tilde{u}' \nabla \cdot \frac{\mathrm{d}f}{\mathrm{d}u}(\bar{u})\right)_Q + \left(w', \frac{\mathrm{d}f}{\mathrm{d}u}(\bar{u}) \nabla \cdot \tilde{u}'\right)_Q \\ & = \left(w', g - \bar{u}_t + \nu \Delta \bar{u} - \nabla \cdot f(\bar{u})\right)_Q = \left(w', \mathcal{R}_{\bar{u}}\right)_Q \qquad \forall w' \in \mathcal{V}^n(0), \end{aligned} \tag{25}$$

where $\tilde{u}'$ is the approximate fine-scale solution and the source term $\mathcal{R}_{\bar{u}}$ on the right-hand side is the residual of the coarse-scale solution. We observe that the left-hand side in (25) is linear with respect to $\tilde{u}'$, such that it can be rewritten as

$$\text{Find } \tilde{u}' \in \mathcal{V}'^n\left(u'(t^n)\right) \text{ s.t.: } \left(w', \mathcal{L}_{\bar{u}} \tilde{u}'\right)_Q = \left(w', \mathcal{R}_{\bar{u}}\right)_Q \qquad \forall w' \in \mathcal{V}^n(0), \tag{26}$$

where the linear differential operator $\mathcal{L}_{\bar{u}}$ corresponds to the differential operator on the left-hand side of (25), assuming $\bar{u}$ is known. Next, we use Green's identities to rewrite the left-hand side term in (26) as

$$\text{Find } \tilde{u}' \in \mathcal{V}'^n\left(u'(t^n)\right) \text{ s.t.: } \quad \left(\mathcal{L}^*_{\bar{u}} w', \tilde{u}'\right)_Q + k(w', \tilde{u}'; \partial Q) = \left(w', \mathcal{R}_{\bar{u}}\right)_Q \qquad \forall w' \in \mathcal{V}^n(0), \tag{27}$$

where $k(\cdot, \cdot; \partial Q)$ is the collection of element interface terms that act on $\partial Q$ and appear as a result of integration by parts, and $\mathcal{L}^*_{\bar{u}}$ is the adjoint of $\mathcal{L}_{\bar{u}}$.

The definition of the Green's function for the linearized PDE at hand is

$$\begin{cases} G(x, y) \in \mathcal{V}^n(0) & \\ \mathcal{L}^*_{\bar{u}} G(x, y) = \delta_x, & \text{for } y \in Q \\ G(x, y) = 0, & \text{for } y \in \partial Q. \end{cases} \tag{28}$$

We choose the Green's function defined in (28) as the test function $w'$. Substituting $G(x, y)$ in place of $w'$ in (27), we obtain

$$\int_Q \mathcal{L}^* G(x, y) \tilde{u}' \, \mathrm{d}y = \int_Q \delta_x \tilde{u}' \, \mathrm{d}y = \tilde{u}' = -k(G(x, y), \tilde{u}'; \partial Q) + \int_Q G(x, y) \mathcal{R}_{\bar{u}} \mathrm{d}y, \tag{29}$$

where the parameter of integration and differentiation is $y$.

Equation (29) is driven by the coarse-scale residual via its last term. It also depends on the fine-scale boundary conditions via the functional $k$. To close the formulation, the fine-scale boundary values $\tilde{u}'$ must be written in terms of the coarse-scale solution, for which the identities in (21) can be used. Since the fine-scale solution $\tilde{u}'$ occurs in the volumetric term in a weighted sense, we can implement all Green's functions as averaged quantities, ie,

$$\left(\mathcal{L}^* \bar{w}, u'\right)_Q \approx \left(\mathcal{L}^* \bar{w}, -k(G(x, y), \tilde{u}'; \partial Q)\right)_Q + \left(\int_Q G(x, y) \mathcal{R}_{\bar{u}} \, \mathrm{d}y\right)_Q \tag{30}$$

$$\approx -\left(\mathcal{L}^* \bar{w}, \sum_{F \in \partial Q} \gamma_F \int_F \left(\Phi - \frac{1}{2} [\![\bar{u}]\!] \cdot n\right)\right)_Q + (\mathcal{L}^* \bar{w}, \tau \mathcal{R}_{\bar{u}})_Q, \tag{31}$$

where $F$ denotes the faces (3D), edges (2D), or nodes (1D) of the element $K$, and $\tau$ and $\gamma_F$ are averaged Green's function quantities. Relation (31) is inspired by the steady advection-diffusion equation with constant coefficients in one dimension, where it is an identity when discretized with linear basis functions. In (31), the averaged Green's function quantities are defined as

$$\tau = \frac{1}{|Q|} \int_Q \int_Q G(x, y) \mathrm{d}y \mathrm{d}x \qquad \gamma_F = \frac{1}{|Q|} \int_Q \int_F \mathcal{G}(x, y) \mathrm{d}y \mathrm{d}x, \tag{32}$$

where $\mathcal{G}$ is a function derived from the Green's function, which depends on the definition of $k$, as we will show for the example of the Burgers equation in the next section.

## 4 | A DG-RVMS FORMULATION FOR THE BURGERS EQUATION

In this section, we apply the general DG-RVMS framework described above to a one-dimensional viscous Burgers equation, which can be obtained from (10) with the following flux function:

$$f(u) = \frac{1}{2} u^2. \tag{33}$$

The space-time finite element setting used in the previous section provides a mathematically rigorous foundation, where the coarse-scale solution can be defined as some projection onto a finite element approximation space in both the temporal and the spatial dimension. In this framework, the volumetric fine-scale model can be defined throughout the whole space-time domain. The resulting model involves all the differential operators, including the time derivative. However, in most practical applications, finite difference schemes are commonly preferred for discretization in time. We therefore switch to a formulation that uses a finite element formulation in space only. In order to use the same volumetric fine-scale

models, we interpret a finite difference step in time from $t^n$ to $t^{n+1}$ as one time slab from the space-time formulation. The new weak formulation is written as

$$\text{Find } u \in \mathcal{W} \text{ s.t.: } \begin{cases} \left(w, u_t - \nu u_{xx} + \frac{1}{2}(u^2)_x\right)_{\Omega_K} = (w, g)_{\Omega_K} & \forall w \in \mathcal{W}(0) \\ [\![u]\!] = 0, & \text{on } \Gamma \\ [\![\nabla u]\!] = 0, & \text{on } \Gamma, \end{cases} \tag{34}$$

where $\mathcal{W}$ is the purely spatial function space equivalence of (11).

## 4.1 | The coarse-scale DG-RVMS system

Using the multiscale split (15) and integration by parts as described in Section 3, we obtain the following coarse-scale weak formulation, analogous to (19):

$$\begin{aligned} &\text{Find } \bar{u} \in \overline{\mathcal{W}} \text{ s.t.:} \\ &\left(\bar{w}, \bar{u}_t + u'_t\right)_{\Omega_K} + \left(\bar{w}_x, \nu \bar{u}_x\right)_{\Omega_K} - \left(\bar{w}_{xx}, \nu u'\right)_{\Omega_K} + \sum_{K \in \mathcal{T}} \left[\langle \bar{w} n, \nu \bar{u}_x \rangle_{\partial K} - \left\langle \bar{w} n, \nu u'_x \right\rangle_{\partial K} - \left\langle \bar{w}_x, \nu u' n \right\rangle_{\partial K}\right] \\ &\quad - \frac{1}{2}\left(\bar{w}_x, \bar{u}^2\right)_{\Omega_K} - \left(\bar{w}_x, \bar{u} u'\right)_{\Omega_K} - \frac{1}{2}\left(\bar{w}_x, u'^2\right)_{\Omega_K} + \sum_{K \in \mathcal{T}} \frac{1}{2}\left\langle \bar{w} n, \left(\bar{u} + u'\right)^2 \right\rangle_{\partial K} = (\bar{w}, f)_{\Omega_K} \quad \forall \bar{w} \in \overline{\mathcal{W}}. \end{aligned} \tag{35}$$

First, we focus on the interface terms that are related to the diffusion term. We substitute the identity (21) and obtain

$$\begin{aligned} &\sum_{K \in \mathcal{T}} \left[\langle \bar{w} n, \nu \bar{u}_x \rangle_{\partial K} - \left\langle \bar{w} n, \nu u'_x \right\rangle_{\partial K} - \langle \bar{w}_x, \nu u' n \rangle_{\partial K}\right] \\ &\quad = \sum_{k \in \mathcal{T}} \left[\langle \bar{w} n, \nu \bar{u}_x \rangle_{\partial K} - \left\langle \bar{w} n, \nu \left\{\!\!\left\{ u'_x \right\}\!\!\right\} \right\rangle_{\partial K} + \left\langle \frac{1}{2} \bar{w}, \nu [\![\bar{u}_x]\!] \right\rangle_{\partial K} + \langle \bar{w}_x n, \nu \{\!\{ u' \}\!\} \rangle_{\partial K} - \left\langle \frac{1}{2} \bar{w}_x, \nu [\![\bar{u}]\!] \right\rangle_{\partial K}\right] \\ &\quad = \sum_{k \in \mathcal{T}} \left[\langle \bar{w} n, \nu \bar{u}_x \rangle_{\partial K}\right] - \left\langle [\![\bar{w}]\!], \nu \left\{\!\!\left\{ u'_x \right\}\!\!\right\} \right\rangle_{\Gamma} + \langle \{\!\{ \bar{w} \}\!\}, \nu [\![\bar{u}_x]\!] \rangle_{\Gamma} + \langle [\![\bar{w}]\!]_x, \nu \{\!\{ u' \}\!\} \rangle_{\Gamma} - \langle \{\!\{ \bar{w}_x \}\!\}, \nu [\![\bar{u}]\!] \rangle_{\Gamma} \\ &\quad = -\left\langle [\![\bar{w}]\!], \nu \left\{\!\!\left\{ u'_x \right\}\!\!\right\} \right\rangle_{\Gamma} - \langle [\![\bar{w}]\!], \nu \{\!\{ \bar{u}_x \}\!\} \rangle_{\Gamma} + \langle [\![\bar{w}]\!]_x, \nu \{\!\{ u' \}\!\} \rangle_{\Gamma} - \langle \{\!\{ \bar{w}_x \}\!\}, \nu [\![\bar{u}]\!] \rangle_{\Gamma}, \end{aligned} \tag{36}$$

where, from the third to the fourth line, we use the following identity:

$$\begin{aligned} &\langle \{\!\{ \bar{w} \}\!\}, [\![\bar{u}_x]\!] \rangle_{\partial K} - \langle \bar{w}, \bar{u}_x n \rangle_{\partial K^+} - \langle \bar{w}, \bar{u}_x n \rangle_{\partial K^-} \\ &\quad = \int_K \left(\frac{1}{2}(\bar{w}^+ + \bar{w}^-)\left(\bar{u}_x^+ n^+ + \bar{u}_x^- n^-\right) - (\bar{w} \bar{u}_x n)^+ - (\bar{w} \bar{u}_x n)^-\right) \\ &\quad = \int_K \frac{1}{2}\left(-\bar{w}^+ n^+ \bar{u}_x^+ - \bar{w}^+ n^+ \bar{u}_x^- - \bar{w}^- n^- \bar{u}_x^+ - \bar{w}^- n^- \nabla \bar{u}^-\right) \\ &\quad = -\int_K \frac{1}{2}(\bar{w}^+ n^+ + \bar{w}^- n^-)\left(\bar{u}_x^- + \bar{u}_x^+\right) = -\langle [\![\bar{w}]\!], \{\!\{ \bar{u}_x \}\!\} \rangle_{\partial K}. \end{aligned} \tag{37}$$

Next, we focus on the interface terms that are related to the nonlinear advective term. Due to the continuity of the true solution $u$, we can infer that $\bar{u} + u' = u$ is single valued on element interfaces. We can therefore write

$$\begin{aligned} \sum_{K \in \mathcal{T}} \frac{1}{2}\left\langle \bar{w} n, \left(\bar{u} + u'\right)^2 \right\rangle_{\partial K} &= \frac{1}{2}\left\langle [\![\bar{w}]\!], u^2 \right\rangle_{\Gamma} = \frac{1}{2}\left\langle [\![\bar{w}]\!], \{\!\{ u \}\!\}^2 \right\rangle_{\Gamma} = \frac{1}{2}\left\langle [\![\bar{w}]\!], \{\!\{ \bar{u} + u' \}\!\}^2 \right\rangle_{\Gamma} \\ &= \frac{1}{2}\left\langle [\![\bar{w}]\!], \left(\{\!\{ \bar{u} \}\!\} + \{\!\{ u' \}\!\}\right)^2 \right\rangle_{\Gamma} = \frac{1}{2}\left\langle [\![\bar{w}]\!], \{\!\{ \bar{u} \}\!\}^2 + 2\{\!\{ \bar{u} \}\!\}\{\!\{ u' \}\!\} + \{\!\{ u' \}\!\}^2 \right\rangle_{\Gamma}. \end{aligned} \tag{38}$$

By substituting the manipulated interface terms of (36) and (38) into (35), we obtain the following coarse-scale weak formulation:

Find $\bar{u} \in \overline{\mathcal{W}}$ s.t.:

$$\begin{aligned}&\left(\bar{w}, \bar{u}_t + u'_t\right)_{\Omega_K} + \left(\bar{w}_x, \nu \bar{u}_x\right)_{\Omega_K} - \left(\bar{w}_{xx}, \nu u'\right)_{\Omega_K} - \langle [\![\bar{w}]\!], \nu \{\!\{ \bar{u}_x \}\!\}\rangle_\Gamma - \langle \{\!\{ \bar{w}_x \}\!\}, \nu [\![\bar{u}]\!]\rangle_\Gamma - \left\langle [\![\bar{w}]\!], \nu \left\{\!\!\left\{ u'_x \right\}\!\!\right\} \right\rangle_\Gamma + \langle [\![\bar{w}_x]\!], \nu \{\!\{ u' \}\!\}\rangle_\Gamma \\ &\quad - \frac{1}{2}\left(\bar{w}_x, \bar{u}^2\right)_{\Omega_K} - \left(\bar{w}_x, \bar{u}\, u'\right)_{\Omega_K} - \frac{1}{2}\left(\bar{w}_x, u'^2\right)_{\Omega_K} + \frac{1}{2}\left\langle [\![\bar{w}]\!], \{\!\{ \bar{u} \}\!\}^2 + 2\{\!\{ \bar{u} \}\!\}\{\!\{ u' \}\!\} + \{\!\{ u' \}\!\}^2 \right\rangle_\Gamma = (\bar{w}, f)_{\Omega_K} \quad \forall \bar{w} \in \overline{\mathcal{W}}. \end{aligned} \tag{39}$$

We emphasize again that no approximations or simplifications have been introduced until this point. This means that the coarse-scale formulation (39) captures the complete multiscale nature of the PDE.

## 4.2 | A fine-scale interface model for the Burgers equation

To eliminate the fine-scale dependencies in the interface terms of (39), we propose the following fine-scale interface model, in reference to (23):

$$\begin{cases} \Phi = \{\!\{ u' \}\!\} = 0, & \text{on } \Gamma \\ \Theta = \left\{\!\!\left\{ u'_x \right\}\!\!\right\} = -(\eta h^{-1} + \frac{1}{2\nu} |\{\!\{ \bar{u} \}\!\}|)\, [\![\bar{u}]\!], & \text{on } \Gamma, \end{cases} \tag{40}$$

where $\eta$ is a model parameter, $h$ is the mesh size, and the viscous-like term $\nu$ is assumed constant.

Substituting the first line of (40) in (39) removes the fine-scale interface term that originates from the Laplace operator and all fine-scale interface terms that originate from the nonlinear advection term. We then substitute the second line of (40) into the remaining fine-scale interface term. We combine the result with the coarse-scale nonlinear advection term as follows:

$$-\left\langle [\![\bar{w}]\!], \nu \left\{\!\!\left\{ u'_x \right\}\!\!\right\} \right\rangle_\Gamma + \frac{1}{2}\left\langle [\![\bar{w}]\!], \{\!\{ \bar{u} \}\!\}^2 \right\rangle_\Gamma = \left\langle [\![\bar{w}]\!], \nu\eta h^{-1} [\![\bar{u}]\!] \right\rangle_\Gamma + \frac{1}{2}\left\langle [\![\bar{w}]\!], \{\!\{ \bar{u} \}\!\} \left( \text{sign}\left(\{\!\{ \bar{u} \}\!\}\right) \frac{1}{2} [\![\bar{u}]\!] + \{\!\{ \bar{u} \}\!\} \right) \right\rangle_\Gamma. \tag{41}$$

The last term in (41) can be manipulated as follows:

$$\begin{aligned} \frac{1}{2}\left\langle [\![\bar{w}]\!], \{\!\{ \bar{u} \}\!\} \left( \text{sign}(\{\!\{ \bar{u} \}\!\}) [\![\bar{u}]\!] + \{\!\{ \bar{u} \}\!\} \right) \right\rangle_\Gamma &= \frac{1}{2}\left\langle [\![\bar{w}]\!], \{\!\{ \bar{u} \}\!\} \left( \text{sign}(\{\!\{ \bar{u} \}\!\}) \frac{1}{2}(\bar{u}^- - \bar{u}^+) + \frac{1}{2}(\bar{u}^- + \bar{u}^+) \right) \right\rangle_\Gamma \\ &= \begin{cases} \frac{1}{2}\langle [\![\bar{w}]\!], \{\!\{ \bar{u} \}\!\} \bar{u}^- \rangle_\Gamma, & \text{if } \{\!\{ \bar{u} \}\!\} > 0 \\ \frac{1}{2}\langle [\![\bar{w}]\!], \{\!\{ \bar{u} \}\!\} \bar{u}^+ \rangle_\Gamma, & \text{if } \{\!\{ \bar{u} \}\!\} < 0 \end{cases} \\ &= \frac{1}{2}\left\langle [\![\bar{w}]\!], \{\!\{ \bar{u} \}\!\} \bar{u} \left( \lim_{\epsilon \to 0} x - \epsilon \{\!\{ \bar{u} \}\!\} \right) \right\rangle_\Gamma, \end{aligned} \tag{42}$$

where at each interface, $\bar{u}^-$ is evaluated on the element on the left and $\bar{u}^+$ is evaluated on the element on the right.

The final coarse-scale variational formulation that we obtain with the fine-scale interface model (40) is

Find $\bar{u} \in \overline{\mathcal{W}}$ s.t.:

$$\begin{aligned}&\left(\bar{w}, \bar{u}_t + u'_t\right)_{\Omega_K} + \left(\bar{w}_x, \nu \bar{u}_x\right)_{\Omega_K} - \left(\bar{w}_{xx}, \nu u'\right)_{\Omega_K} - \langle [\![\bar{w}]\!], \nu \{\!\{ \bar{u}_x \}\!\}\rangle_\Gamma - \langle \{\!\{ \bar{w}_x \}\!\}, \nu [\![\bar{u}]\!]\rangle_\Gamma + \left\langle [\![\bar{w}]\!], \eta h^{-1} \nu [\![\bar{u}]\!] \right\rangle_\Gamma \\ &\quad - \frac{1}{2}\left(\bar{w}_x, \bar{u}^2\right)_{\Omega_K} - \left(\bar{w}_x, \bar{u}\, u'\right)_{\Omega_K} - \frac{1}{2}\left(\bar{w}_x, u'^2\right)_{\Omega_K} + \frac{1}{2}\left\langle [\![\bar{w}]\!], \{\!\{ \bar{u} \}\!\} \bar{u} \left( \lim_{\epsilon \to 0} x - \epsilon \{\!\{ \bar{u} \}\!\} \right) \right\rangle_\Gamma = (\bar{w}, f)_{\Omega_K} \quad \forall \bar{w} \in \overline{\mathcal{W}}. \end{aligned} \tag{43}$$

Our DG-RVMS formulation originates completely from a VMS point of view. It is interesting to note, however, that it features components that closely resemble classical DG formulations. For example, the fine-scale interface model can be interpreted as combining an IP treatment of the diffusion term with an upwinding treatment of the advective term. For the upwind method, an advective velocity of magnitude $u = \{\!\{ \bar{u} \}\!\}$ is used. Therefore, the DG-RVMS point of view offers a multiscale interpretation of classical formulations. In particular, we may conclude that when the fine-scale volume terms are treated appropriately, the use of an IP method combined with an upwind method implicitly enforces a projector that corresponds to the fine-scale interface model (40). We refer the interested reader to our earlier work,[33] where we studied the nature of this projector in more detail.

## 4.3 | A fine-scale volumetric model for the Burgers equation

To eliminate the fine-scale dependencies in the volumetric terms of (39), we derive a volumetric fine-scale model based on the space-time fine-scale weak formulation described in Section 3.3. We note that we neglect the fine-scale time derivative

in the first term of (43), which is common practice.[5] For the one-dimensional case, we develop a fine-scale volumetric model of the form

$$u' \approx \tau \mathcal{R}_{\bar{u}} + \frac{1}{2}\gamma_0 [\![\bar{u}]\!]\Big|_{x_j} - \frac{1}{2}\gamma_1 [\![\bar{u}]\!]\Big|_{x_{j+1}}, \tag{44}$$

where the point $x_j$ corresponds to the left node of the current element in which $u'$ is to be modeled, and $x_{j+1}$ to the right node. We observe that relation (44) corresponds to (31), with the fine-scale interface model $\Phi$ from (40).

We obtain the definitions of $\tau$, $\gamma_0$, and $\gamma_1$ from the fine-scale problem. Following the residual-based strategy described in Section 3.3, the fine-scale problem can be written as

$$\text{Find } \tilde{u}' \in \mathcal{V}'(0) \text{ s.t.: } \quad \left(w', \tilde{u}'_t - \nu \tilde{u}'_{xx} + \bar{u}_x \tilde{u}' + \bar{u}\tilde{u}'_x\right)_Q = \left(w', \mathcal{R}_{\bar{u}}\right)_Q \qquad \forall w' \in \mathcal{V}(0). \tag{45}$$

Thereby, we may define the linearized fine-scale differential operator, its adjoint, and the accompanying interface integrals as

$$\begin{aligned} \mathcal{L} &= \frac{\mathrm{d}}{\mathrm{d}t} + \bar{u}_x + \bar{u}\frac{\mathrm{d}}{\mathrm{d}x} - \nu\frac{\mathrm{d}^2}{\mathrm{d}x^2} \\ \mathcal{L}^* &= -\frac{\mathrm{d}}{\mathrm{d}t} + \bar{u}_x - \bar{u}\frac{\mathrm{d}}{\mathrm{d}x} - \nu\frac{\mathrm{d}^2}{\mathrm{d}x^2} \\ k(w', u'; \partial Q) &= -\langle w', u' \rangle_{\partial Q_{t^n}} + \langle w', u' \rangle_{\partial Q_{t^{n+1}}} + \langle w' n, \bar{u} u' \rangle_{\partial Q_x} - \left\langle w' n, \nu u'_x \right\rangle_{\partial Q_x} + \left\langle w'_x, \nu u' n \right\rangle_{\partial Q_x}, \end{aligned} \tag{46}$$

where $\partial Q_{t^n}$ refers to the temporal boundary of $\partial Q$, and $\partial Q_x$ to the spatial boundary, as defined in Table 1.

We construct the parameter $\tau$ associated to the Burgers equation by means of asymptotic scaling arguments. The behavior of the PDE depends on the set of parameters $\nu$, $\bar{u}_x$, and $\bar{u}$. Their values determine which differential operators dominate the collective $\tau$. We expect the following asymptotic behavior:

$$\begin{aligned} 1 \gg \nu, \bar{u}_x, \bar{u} \quad &\Rightarrow \quad \tau \to \tau_t = \frac{(t^{n+1} - t^n)^2}{2h} C_1^{q-1} \\ \bar{u}_x \gg 1, \nu, \bar{u} \quad &\Rightarrow \quad \tau \to \tau_R = \frac{1}{\bar{u}_x} C_2^{p-1} \\ \bar{u} \gg 1, \bar{u}_x, \nu \quad &\Rightarrow \quad \tau \to \tau_A = \frac{h}{2\bar{u}} C_2^{p-1} \\ \nu \gg 1, \bar{u}, \bar{u}_x \quad &\Rightarrow \quad \tau \to \tau_D = \frac{h^2}{12\nu} C_2^{p-1}, \end{aligned} \tag{47}$$

where $\tau_t$ corresponds to the Green's function of a purely temporal differential operator $\frac{\mathrm{d}}{\mathrm{d}t}$. Similarly, $\tau_R$, $\tau_A$, and $\tau_D$ correspond to the reactive, advective, and diffusive components, respectively. Explicit expressions for these Green's function quantities are derived in the Appendix. These expressions are suitable for both uniform and nonuniform meshes due to their element-local derivation.

We add factors $C_1^{q-1}$ and $C_2^{p-1}$ to mitigate the averaging error introduced in (31) when using higher-order basis functions. Here, $p$ and $q$ denote the polynomial degree of the finite element discretization and the convergence rate of the finite difference time integration method. We note that coefficients $C_1$ and $C_2$ should be smaller than 1 to enable convergence. In our numerical experiments, however, we found that larger values sometimes yield better results.

The final $\tau$ is constructed from the single components in (47) as follows:

$$\tau = \frac{1}{\sqrt{\left(\frac{1}{\tau_t}\right)^2 + \left(\frac{1}{\tau_R}\right)^2 + \left(\frac{1}{\tau_A}\right)^2 + \left(\frac{1}{\tau_D}\right)^2}}, \tag{48}$$

where we follow the asymptotic scaling argument that is commonly used to derive stabilization parameters in stabilized finite element methods.[39]

The definition of $\gamma$ can be based on the interface integrals in (46), where we replace the test function $w'$ by the Green's function. Since the Green's function is, by definition, zero on the element boundaries, only the last term remains. Comparing this term to the definition of $\gamma$ in (32), we find

$$\mathcal{G}(x, y) = \nu \frac{\mathrm{d}}{\mathrm{d}y} G(x, y). \tag{49}$$

Similar to the construction of $\tau$, a $\gamma$ expression can be derived for each differential operator (temporal, reactive, advective, and diffusive). As shown in the Appendix, for the present case, only the $\gamma$ that corresponds to the diffusion operator is nonzero. In our numerical experiments, we will use

$$\gamma_0 = \frac{1}{2\nu} C_3$$
$$\gamma_1 = -\frac{1}{2\nu} C_3. \tag{50}$$

We introduce another factor, $C_3$, for the same reason as above, ie, to mitigate the averaging error.

## 5 | NUMERICAL EXPERIMENTS

In this section, we will illustrate the potential of the DG-RVMS formulation and the associated fine-scale models to improve the accuracy of the finite element solution by incorporating subgrid-scale behavior of the one-dimensional Burgers model problem. To this end, we return to the Burgers benchmark that we introduced in Section 2.3 and whose solution and energy spectra are plotted in Figure 3. We use the result of the DNS discretization presented in Section 2.3 as the reference solution. Our DG-RVMS formulation is based on (43), with the volumetric fine-scale model derived in Section 4.3. We use the classical explicit time-accurate fourth-order Runge-Kutta method (RK4) for time integration, where we interpret the time-step $t^n \rightarrow t^{n+1}$ as a time slab in the volumetric fine-scale model. The RK4 algorithm produces a solution $\bar{u}$ at $t^{n+1}$ based on the known solution at $t^n$ and a weighted average of intermediate time derivatives. The intermediate time derivatives are obtained from the coarse-scale formulation, where we use the solution $\bar{u}$ of the previous intermediate computation for the explicit treatment of all coarse-scale terms. This includes the residual and interface jumps in the volumetric fine-scale model (44). The following numerical experiments use a time-step size of $\Delta t = \pi/(8pN)$, where $p$ is the polynomial order of the DG basis functions and $N$ is the total number of elements. The RK4 method is fourth-order accurate in terms of the total accumulated error but fifth-order accurate in terms of the local truncation error, and hence, $q = 5$ in (47).

In these numerical experiments, we compare three different DG formulations. These are the "No volumetric model" formulation, the "CG-RVMS" formulation, and the "DG-RVMS" formulation. Their finite element schemes are devised as follows.

- No volumetric model: This scheme still uses the fine-scale interface model (40) to couple the elements. The volumetric model derived in Section 4.3 is completely omitted. Effectively, this reduces to a DG formulation with an IP treatment of the diffusive term and an upwind treatment of the advective term.
- CG-RVMS: This formulation adds the classical residual-based fine-scale model onto the "No volumetric model" scheme. This only concerns the $\tau$-term in (44). Consequently, it is implicitly assumed that the fine-scales vanish on element boundaries.
- DG-RVMS: This formulation makes use of the complete model (44). In contrast to the above models, we also incorporate the effect of the nonvanishing fine-scale element boundary values in the volumetric residual-based fine-scale model.

As a final note regarding these formulations, we would like to emphasize once more that the CG-RVMS model represents the current standard in turbulence modeling in the finite element framework. It is widely adopted in isogeometric or continuous Galerkin finite element computations. It will thus be the benchmark subgrid-scale model that we use to determine the effectiveness of the DG-RVMS variant proposed herein. For an overview of other subgrid-scales, we refer the reader to the work of Li and Wang.[40]

### 5.1 | Accuracy in solution fields

Figures 5-7 show the resulting solutions at times $t = 7.75\pi$ and $t = 8\pi$, obtained with four DG elements and higher-order basis functions of polynomial order $p = 2$, $p = 3$, and $p = 4$, respectively. At time $t = 7.75\pi$, the wave front lies in the center of an element, and at time $t = 8\pi$, it lies in between two elements.

The residual-based fine-scale model that corresponds to the "CG-RVMS" solution made use of the constants $C_1 = 3$ and $C_2 = 0.7$. The residual-based model that corresponds to the "DG-RVMS" solution uses the same constants $C_1 = 3$ and $C_2 = 0.7$. It also includes the newly introduced jump terms in formulation (44), where the additional coefficient

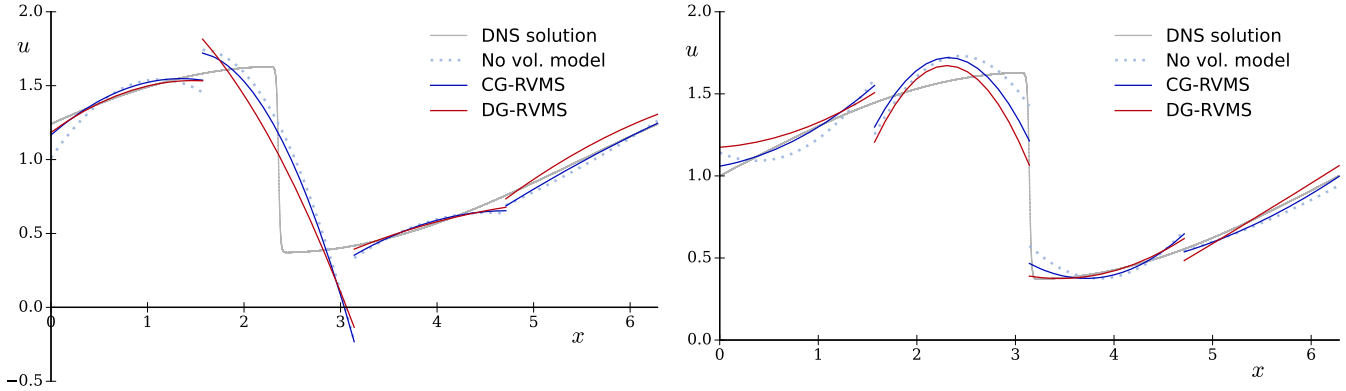


**(A)** At $t = 7.75\pi$ **(B)** At $t = 8\pi$

**FIGURE 5** Example solutions with and without the proposed discontinuous Galerkin residual-based variational multiscale (DG-RVMS) model, using four discontinuous Galerkin elements of $p = 2$. A, At $t = 7.75\pi$; B, At $t = 8\pi$. CG-RVMS, continuous Galerkin residual-based variational multiscale; DNS, direct numerical simulation [Colour figure can be viewed at wileyonlinelibrary.com]

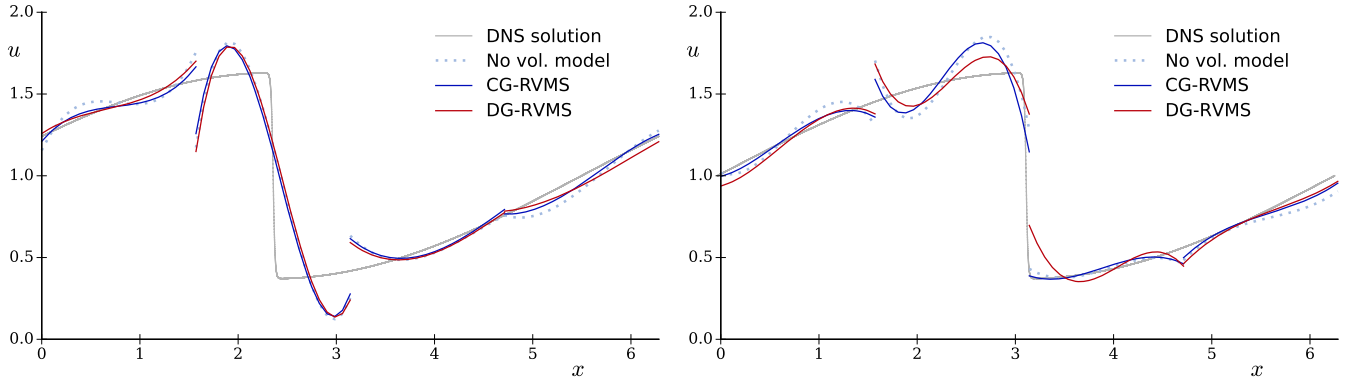


**(A)** At $t = 7.75\pi$ **(B)** At $t = 8\pi$

**FIGURE 6** Example solutions with and without the proposed discontinuous Galerkin residual-based variational multiscale (DG-RVMS) model, using four discontinuous Galerkin elements of $p = 3$. A, At $t = 7.75\pi$; B, At $t = 8\pi$. CG-RVMS, continuous Galerkin residual-based variational multiscale; DNS, direct numerical simulation [Colour figure can be viewed at wileyonlinelibrary.com]

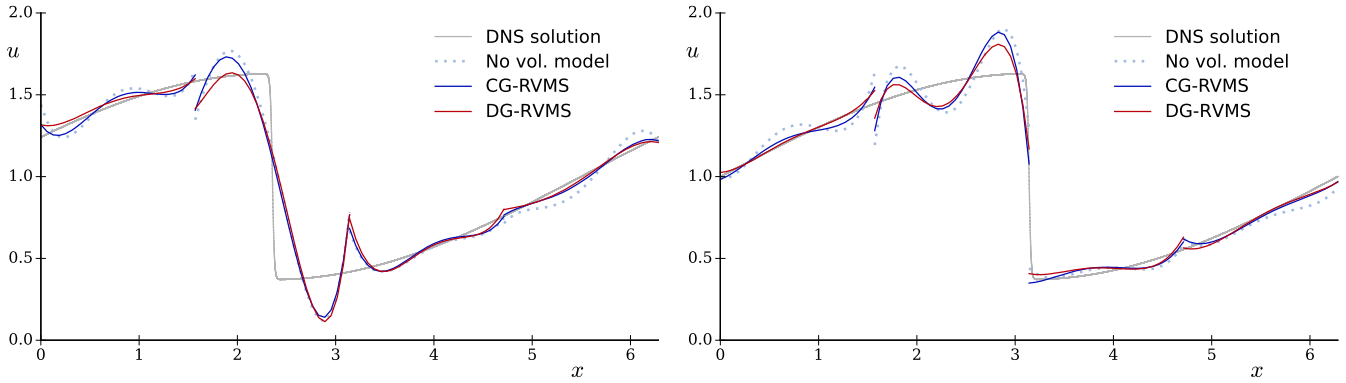


**(A)** At $t = 7.75\pi$ **(B)** At $t = 8\pi$

**FIGURE 7** Example solutions with and without the proposed discontinuous Galerkin residual-based variational multiscale (DG-RVMS) model, using four discontinuous Galerkin elements of $p = 4$. A, At $t = 7.75\pi$; B, At $t = 8\pi$. CG-RVMS, continuous Galerkin residual-based variational multiscale; DNS, direct numerical simulation [Colour figure can be viewed at wileyonlinelibrary.com]

is $C_3 = 0.3$. Each Figure compares the RVMS solutions to the DNS reference solution and the "No volumetric model" solution. We observe that with respect to the DNS reference, the RVMS formulation consistently improves the accuracy of the solution. The oscillations within the elements become smaller, and the jumps from element to element decrease. We observe that the CG-RVMS solution is slightly less accurate than the DG-RVMS solution.

## 5.2 | Convergence of kinetic energy

As shown in Figures 5-7, the DG method that excludes a volumetric model is already performing very well by itself due to the simplicity of the model problem. Hence, the quality of the solution field itself is not the most appropriate indicator for the performance of the DG-RVMS method. In Section 2, we reviewed the scale interaction in the Burgers equation, which revolves around the transfer of energy between coarse-scale and fine-scale solution components. We can therefore expect that the error in the total kinetic energy, as defined in (8), is a much more adequate measure for the performance of the DG-RVMS method and its associated fine-scale models.

In the following, we examine the convergence of the relative total kinetic energy of the solution at time $t = 8\pi$, when the DG discretization in space is uniformly refined. The relative energy is computed with respect to the energy of the DNS solution averaged over the time window $6\pi \leq t \leq 8\pi$, where the wave form of the solution is steady.

We perform three sets of experiments to assess the energy convergence of the DG-RVMS formulation, which we report in Figures 8-10 for DG meshes of polynomial order $p = 2$, $p = 3$, and $p = 4$, respectively. In each Figure, we plot the energy errors that were obtained with the DG-RVMS model and the CG-RVMS model ($C_3 = 0$) and without a volumetric fine-scale model.

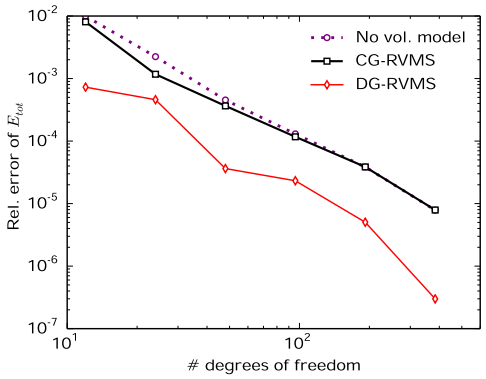


| | Model 1 | | Model 2 | |
|---|---|---|---|---|
| Dofs | $C_{1\&2}$ | $C_3$ | $C_1$ | $C_2$ |
| 12 | 0.7 | 0.1 | 3.0 | 0.7 |
| 24 | 0.7 | 0.1 | 3.0 | 0.7 |
| 48 | 0.7 | 0.1 | 2.0 | 0.7 |
| 96 | 0.7 | 0.1 | 2.0 | 0.7 |
| 192 | 0.7 | 0.1 | 0.7 | 0.7 |
| 384 | 0.7 | 0.1 | 0.7 | 0.7 |

**FIGURE 8** Energy convergence with uniform mesh refinement at $t = 8\pi$ for basis functions of $p = 2$. CG-RVMS, continuous Galerkin residual-based variational multiscale; DG-RVMS, discontinuous Galerkin residual-based variational multiscale; Dofs, degrees of freedom [Colour figure can be viewed at wileyonlinelibrary.com]

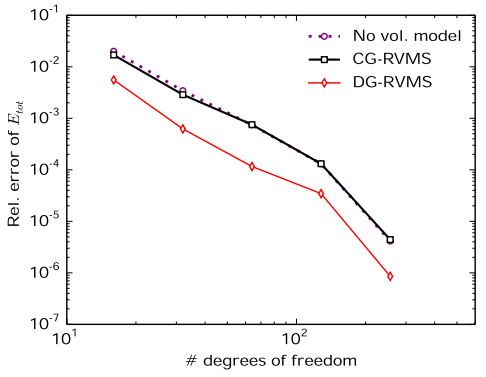


| | Model 1 | | Model 2 | |
|---|---|---|---|---|
| Dofs | $C_{1\&2}$ | $C_3$ | $C_1$ | $C_2$ |
| 16 | 0.7 | 0.3 | 3.0 | 0.7 |
| 32 | 0.7 | 0.2 | 3.0 | 0.7 |
| 64 | 0.7 | 0.2 | 2.0 | 0.7 |
| 128 | 0.7 | 0.1 | 0.7 | 0.7 |
| 256 | 0.7 | 0.025 | 0.7 | 0.7 |

**FIGURE 9** Energy convergence with uniform mesh refinement at $t = 8\pi$ for basis functions of $p = 3$. CG-RVMS, continuous Galerkin residual-based variational multiscale; DG-RVMS, discontinuous Galerkin residual-based variational multiscale; Dofs, degrees of freedom [Colour figure can be viewed at wileyonlinelibrary.com]

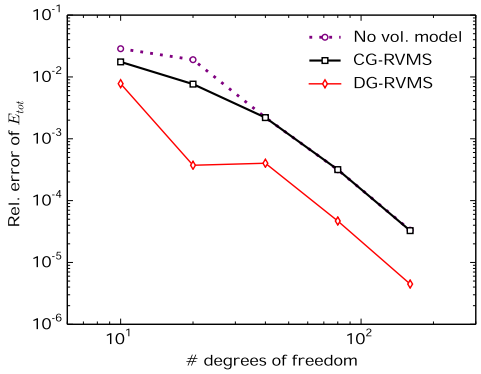


| | Model 1 | | Model 2 | |
|---|---|---|---|---|
| Dofs | $C_{1\&2}$ | $C_3$ | $C_1$ | $C_2$ |
| 10 | 0.7 | 0.3 | 3.0 | 0.7 |
| 20 | 0.7 | 0.3 | 3.0 | 0.7 |
| 40 | 0.7 | 0.3 | 2.0 | 0.7 |
| 80 | 0.7 | 0.3 | 0.7 | 0.7 |
| 160 | 0.7 | 0.025 | 0.7 | 0.7 |

**FIGURE 10** Energy convergence with uniform mesh refinement at $t = 8\pi$ for basis functions of $p = 4$. CG-RVMS, continuous Galerkin residual-based variational multiscale; DG-RVMS, discontinuous Galerkin residual-based variational multiscale; Dofs, degrees of freedom [Colour figure can be viewed at wileyonlinelibrary.com]

Each of the Figures is complemented by a table that shows the coefficients that were used at different mesh resolutions. For the DG-RVMS case, coefficients $C_1$ and $C_2$ were kept at a constant value of 0.7, whereas coefficient $C_3$ was optimized empirically. For the CG-RVMS case, coefficient $C_2$ was kept at 0.7, and coefficient $C_1$ was optimized empirically. Generally, the optimal value for the coefficients was found to decrease with mesh refinement.

We observe that the DG-RVMS method is able to decrease the relative energy error of the solution by almost one order of magnitude with respect to the DG method without a volumetric fine-scale model. The three Figures confirm that the improvement in energy accuracy occurs consistently for the complete range of mesh sizes and for all polynomial orders examined. It is interesting to see that the CG-RVMS model does not improve the energy accuracy. This indicates that the fine-scale boundary values included in the fine-scale volumetric model as proposed in Section 3.3 play a pivotal role for the optimal performance of the DG-RVMS formulation.

## 5.3 | Accuracy of energy spectra

As a final measure of accuracy, we plot the energy spectra for a set of solutions. As discussed in Section 2, we can obtain these spectra by means of a fast Fourier transform that transfers a solution field from its spatial representation to its frequency domain. The number of interpolation points that are used for the transform is twice the number of degrees of freedom. Frequencies higher than that purely capture the piecewise polynomial nature of the solution field, leading to overlapping curves for the solutions with or without the volumetric model. We average the energy spectra over the time window $6\pi \leq t \leq 8\pi$, where the wave form of the solution is steady. We perform this analysis for models that include, and exclude, the DG-RVMS fine-scale volumetric model. Figures 11-13 plot the energy spectra and the associated error

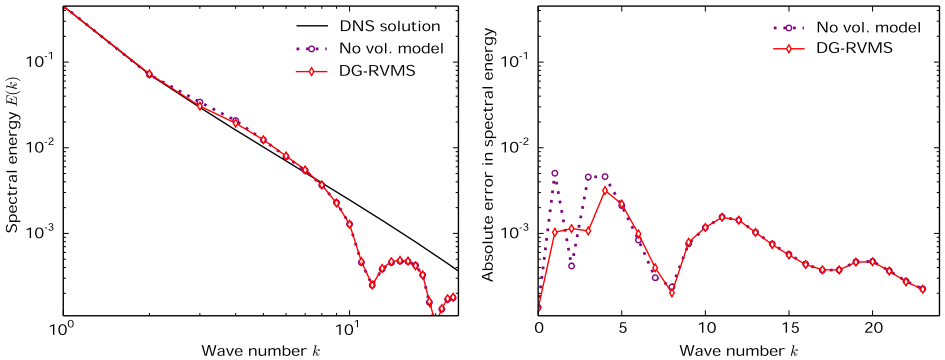


**(A)** Spectra. **(B)** Absolute error.

**FIGURE 11** Spectral energy obtained with eight discontinuous Galerkin elements of $p = 2$ and 24 degrees of freedom. A, Spectra; B, Absolute error. DG-RVMS, discontinuous Galerkin residual-based variational multiscale; DNS, direct numerical simulation [Colour figure can be viewed at wileyonlinelibrary.com]

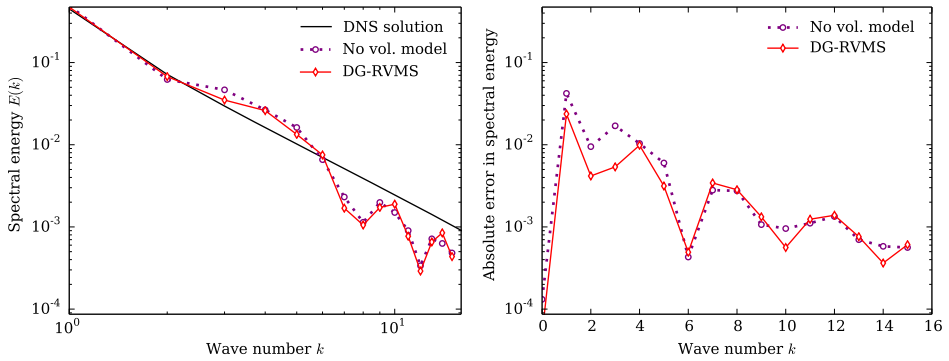


**(A)** Spectra. **(B)** Absolute error.

**FIGURE 12** Spectral energy obtained with four discontinuous Galerkin elements of $p = 3$ and 16 degrees of freedom. A, Spectra; B, Absolute error. DG-RVMS, discontinuous Galerkin residual-based variational multiscale; DNS, direct numerical simulation [Colour figure can be viewed at wileyonlinelibrary.com]

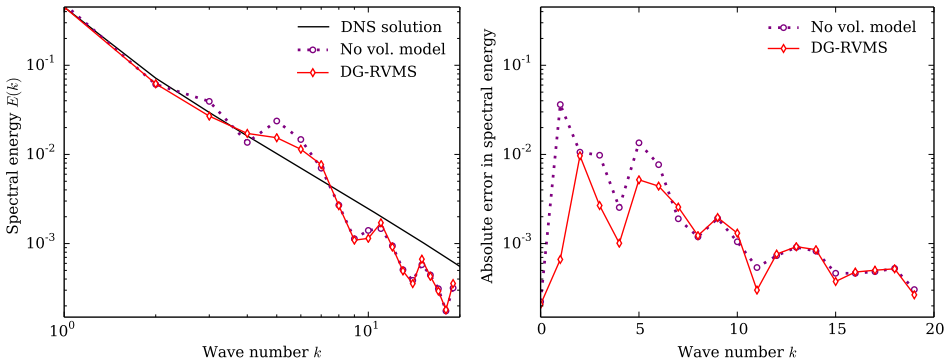


**(A)** Spectra. **(B)** Absolute error.

**FIGURE 13** Spectral energy obtained with four discontinuous Galerkin elements of $p = 4$ and 20 degrees of freedom. A, Spectra; B, Absolute error. DG-RVMS, discontinuous Galerkin residual-based variational multiscale; DNS, direct numerical simulation [Colour figure can be viewed at wileyonlinelibrary.com]

for each wave number for three coarse meshes of polynomial degree $p = 2$, $p = 3$, and $p = 4$, respectively. The error in the spectra is computed with respect to the spectrum of the DNS solution averaged over the time window $6\pi \leq t \leq 8\pi$.

We observe that the DG-RVMS method consistently performs better than the variant that excludes the volumetric fine-scale model. This improvement occurs primarily in the low-frequency range, where the spectral energy is significantly closer to the DNS reference spectrum.

This observation confirms that the DG-RVMS formulation reduces the spurious energy buildup in the low-frequency modes. This issue was discussed in the work of Hulshoff[38] for discretization schemes without a subgrid-scale model in the context of the one-dimensional Burgers equation. Comparing the errors in Figures 11-13, we see that the DG-RVMS formulation becomes more effective for higher-order DG discretizations.

## 6 | SUMMARY, CONCLUSIONS, AND OUTLOOK

In this paper, we extended the DG-RVMS method to nonlinear hyperbolic problems. Our method is based on the decomposition of the solution into coarse-scale and fine-scale components in each DG element, while using multiscale-type transmission conditions to tie discontinuous elements together. We showed that the effect of the fine scales on the coarse-scale part of the weak formulation manifests itself in the form of two types of fine-scale terms, which we classified as fine-scale volumetric terms and fine-scale interface terms.

For the one-dimensional Burgers equation, we closed the formulation on the coarse-scale level by devising suitable fine-scale models that can replace the exact, but unknown, fine-scale volumetric and interface terms. With our fine-scale

models, we naturally obtained an IP-type treatment of the viscous term and an upwind-type treatment of the advective term. The fine-scale volumetric model proposed in this paper incorporates nonhomogeneous fine-scale boundary values, which appear as volumetric integrals of the jump of the coarse-scale solution across element interfaces. We emphasize that our fine-scale models do not use any ad hoc devices such as eddy viscosities. All the models that we propose are consistent and inspired mathematically by the fine-scale equation rather than phenomenologically. The parameters that remain are understood in terms of their mathematical interpretation and their potential range of values.

Our numerical experiments with the one-dimensional Burgers equation demonstrate that our DG-RVMS formulation and the associated fine-scale models can represent the energy dissipation mechanism of the Burgers problem at very coarse meshes, when the dissipative high-frequency modes are unresolved. The solutions of our DG-RVMS method reduce the error of the total kinetic energy by approximately one order of magnitude compared to a DG method without a volumetric subgrid-scale model. By investigating the resulting energy spectra, we showed that the added dissipation targets the correct wave modes. We also showed that the improved energy accuracy is predominantly the effect of the new jump term in the volumetric fine-scale model, which indicates that this fine-scale model truly incorporates a missing subgrid-scale component in the formulation.

The quality of the DG-RVMS results indicates that our new fine-scale models constitute an adequate subgrid-scale model for the Burgers equation. On the basis of the similarities in kinetic energy transport and dissipation in the Burgers and Navier-Stokes cascades, one can anticipate that the improved consistency in representing the effects of unresolved scales provided by the current DG-RVMS approach makes it an attractive candidate for application to the LES of turbulent flows in the context of higher-order DG methods.

## ACKNOWLEDGEMENT

D. Schillinger gratefully acknowledges support from the National Science Foundation through NSF CAREER Award 1651577.

## ORCID

*Stein K.F. Stoter* http://orcid.org/0000-0001-5845-4900

## REFERENCES

1. Hughes TJR. Multiscale phenomena: Green's functions, the Dirichlet-to-Neumann formulation, subgrid scale models, bubbles and the origins of stabilized methods. *Comput Methods Appl Mech Eng*. 1995;127(1-4):387-401.
2. Hughes TJR, Feijóo GR, Mazzei L, Quincy J-B. The variational multiscale method—a paradigm for computational mechanics. *Comput Methods Appl Mech Eng*. 1998;166(1-2):3-24.
3. Hughes TJR, Stewart JR. A space-time formulation for multiscale phenomena. *J Comput Appl Math*. 1996;74(1-2):217-229.
4. Bazilevs Y. Isogeometric analysis of turbulence and fluid-structure interaction [PhD thesis]. Austin, TX: The University of Texas at Austin; 2006.
5. Bazilevs Y, Calo VM, Cottrell JA, Hughes TJR, Reali A, Scovazzi G. Variational multiscale residual-based turbulence modeling for large eddy simulation of incompressible flows. *Comput Methods Appl Mech Eng*. 2007;197(1-4):173-201.
6. Calo VM. Residual-based multiscale turbulence modeling: finite volume simulations of bypass transition [PhD thesis]. Stanford, CA: Stanford University; 2004.
7. Kamensky D, Hsu M-C, Schillinger D, et al. An immersogeometric variational framework for fluid-structure interaction: application to bioprosthetic heart valves. *Comput Methods Appl Mech Eng*. 2015;284:1005-1053.
8. Brezzi F, Franca LP, Hughes TJR, Russo A. $b = \int G$. *Comput Meth Appl Mech Eng*. 1997;145;(3):329-339.
9. Donea J, Huerta A. *Finite Element Methods for Flow Problems*. Hoboken, NJ: John Wiley & Sons; 2003.
10. Hughes TJR, Scovazzi G, Franca LP. Multiscale and stabilized methods. In: Stein E, de Borst R, Hughes TJR, eds. *Encyclopedia of Computational Mechanics*. Hoboken, NJ: John Wiley & Sons; 2004:1-64.
11. Mavriplis D, Nastase C, Shahbazi K, Wang L, Burgess N. Progress in high-order discontinuous Galerkin methods for aerospace applications. Paper presented at: 47th AIAA Aerospace Sciences Meeting including the New Horizons Forum and Aerospace Exposition; 2009; Orlando, FL.
12. Wang ZJ, Fidkowski K, Abgrall R, et al. High-order CFD methods: current status and perspective. *Int J Numer Methods Fluids*. 2013;72(8):811-845.
13. Cockburn B, Karniadakis GE, Shu C-W. *Discontinuous Galerkin Methods: Theory, Computation and Applications*. Berlin, Germany: Springer-Verlag Berlin Heidelberg; 2000.

14. Arnold DN, Brezzi F, Cockburn B, Marini LD. Unified analysis of discontinuous Galerkin methods for elliptic problems. *SIAM J Numer Anal*. 2002;39(5):1749-1779.
15. Peraire J, Persson P-O. The compact discontinuous Galerkin (CDG) method for elliptic problems. *SIAM J Sci Comput*. 2008;30(4):1806-1824.
16. Hartmann R. Numerical analysis of higher order discontinuous Galerkin finite element methods. In: Deconinck H, ed. *35th CFD/ADIGMA Course on Very High Order Discretization Methods*. Sint-Genesius-Rode, Belguim: von Karman Institute for Fluid Dynamics; 2008:1-107. *VKI LS*.
17. Kirby RM, Sherwin SJ, Cockburn B. To CG or to HDG: a comparative study. *J Sci Comput*. 2012;51(1):183-212.
18. Huerta A, Angeloski A, Roca X, Peraire J. Efficiency of high-order elements for continuous and discontinuous Galerkin methods. *Int J Numer Methods Eng*. 2013;96(9):529-560.
19. Lehrenfeld C, Schöberl J. High order exactly divergence-free hybrid discontinuous Galerkin methods for unsteady incompressible flows. *Comput Methods Appl Mech Eng*. 2016;307:339-361.
20. Bochev P, Hughes TJR, Scovazzi G. A multiscale discontinuous Galerkin method. In: Lirkov I, Margenov S, Waśniewski J, eds. *Large-Scale Scientific Computing: 5th International Conference, LSSC 2005, Sozopol, Bulgaria, June 6-10, 2005. Revised Papers*. Berlin, Germany: Springer-Verlag Berlin Heidelberg ; 2005;84-93.
21. Buffa A, Hughes TJR, Sangalli G. Analysis of a multiscale discontinuous Galerkin method for convection-diffusion problems. *SIAM J Numer Anal*. 2006;44(4):1420-1440.
22. Hughes TJR, Scovazzi G, Bochev PB, Buffa A. A multiscale discontinuous Galerkin method with the computational structure of a continuous Galerkin method. *Comput Methods Appl Mech Eng*. 2006;195(19-22):2761-2787.
23. Coley C, Evans JA. Variational multiscale modeling with discontinuous subscales: analysis and application to scalar transport. arXiv preprint arXiv:1705.00082; 2017.
24. Sangalli G. A discontinuous residual-free bubble method for advection-diffusion problems. *J Eng Math*. 2004;49(2):149-162.
25. Collis SS. The DG/VMS method for unified turbulence simulation. Paper presented at: 32nd AIAA Fluid Dynamics Conference and Exhibit; 2002; St. Louis, MO.
26. Collis SS, Ramakrishnan S. The local variational multiscale method. Paper presented at: Third MIT Conference on Computational Fluid and Solid Dynamics; 2005; Cambridge, MA.
27. Ramakrishnan S, Collis SS. Turbulence control simulation using the variational multiscale method. *AIAA J*. 2004;42(4):745-753.
28. Kuru G, de la Llave Plata M, Couaillier V, Abgrall R, Coquel F. An adaptive variational multiscale discontinuous Galerkin method for large eddy simulation. Paper presented at: 54th AIAA Aerospace Sciences Meeting; 2016; San Diego, CA.
29. Beck AD, Flad DG, Tonhäuser C, Gassner G, Munz C-D. On the influence of polynomial de-aliasing on subgrid scale models. *Flow Turbul Combust*. 2016;97(2):475-511.
30. Frère A, de Wiart CC, Hillewaert K, Chatelain P, Winckelmans G. Application of wall-models to discontinuous Galerkin LES. *Phys Fluids*. 2017;29(8): Article ID 085111.
31. Krank B, Kronbichler M, Wall WA. Wall modeling via function enrichment within a high-order DG method for RANS simulations of incompressible flow. *Int J Numer Methods Fluids*. 2018;86:107-129.
32. Akkerman I, Bazilevs Y, Calo VM, Hughes TJR, Hulshoff S. The role of continuity in residual-based variational multiscale modeling of turbulence. *Comput Mech*. 2008;41(3):371-378.
33. Stoter SKF, Turteltaub SR, Hulshoff SJ, Schillinger D. Residual-based variational multiscale modeling in a discontinuous Galerkin framework. *SIAM Multiscale Modeling & Simulation*. arXiv:1709.03934v2 [math.NA]; 2018.
34. Bec J, Khanin K. Burgers turbulence. *Phys Rep*. 2007;447(1-2):1-66.
35. Tsinober A. *An Informal Introduction to Turbulence*. Berlin, Germany: Springer-Verlag Berlin Heidelberg; 2009. *Fluid Mechanics and Its Applications*; Vol. 92.
36. Moreno CG. Turbulence, Vibrations, Noise and Fluid Instabilities. Practical Approach. In: Oh HW, ed. *Computational Fluid Dynamics*. Vukovar, Croatia: Intech; 2010:103-132.
37. Kolmogorov AN. Dissipation of energy in the locally isotropic turbulence. *Proc Math Phys Sci*. 1941;434(1890):15-17.
38. Hulshoff SJ. Implicit subgrid-scale models in space-time variational-multiscale discretizations. *Int J Numer Methods Fluids*. 2005;47(10-11):1093-1099.
39. Tezduyar TE. Stabilized finite element formulations for incompressible flow computations. *Adv Appl Mech*. 1991;28(C):1-44.
40. Li Y, Wang ZJ. A priori and a posteriori evaluations of sub-grid scale models for the Burgers' equation. *Comput Fluids*. 2016;139:92-104.


**How to cite this article:** Stoter SKF, Turteltaub SR, Hulshoff SJ, Schillinger D. A discontinuous Galerkin residual-based variational multiscale method for modeling subgrid-scale behavior of the viscous Burgers equation. *Int J Numer Meth Fluids*. 2018;88:217–238. https://doi.org/10.1002/fld.4662

## APPENDIX

### GREEN'S FUNCTIONS AND $\tau$ AND $\gamma$ EXPRESSIONS

In this Appendix, we derive Green's functions for the differential diffusion, advection, and reaction operators that are involved in the linearized fine-scale problem associated with the Burgers equation. We also derive the corresponding expressions for $\tau$ and $\gamma$.

## A.1 | Diffusion operator

$$\mathcal{L} = -\nu\Delta \qquad \mathcal{L}^* = -\nu\Delta$$

The Green's function for a one-dimensional diffusion operator is defined as

$$\begin{cases} -\nu\frac{\mathrm{d}^2}{\mathrm{d}y^2}G(x,y) = \delta_x, & \text{for } y \in (x_j, x_{j+1}) \\ G(x,y) = 0, & \text{for } y \in \{x_j, x_{j+1}\}. \end{cases} \tag{A1}$$

We integrate the first line and obtain a step function of magnitude $-\nu^{-1}$, as follows:

$$\frac{\mathrm{d}}{\mathrm{d}x}G(x,y) = \begin{cases} C_1, & \text{when } y < x \\ C_1 - \frac{1}{\nu}, & \text{when } y \geq x. \end{cases} \tag{A2}$$

Further integration results in a Green's function that is piecewise linear. The slope is defined according to (A2). The following structure also satisfies the boundary conditions:

$$G(x,y) = \begin{cases} g_1(x,y) = C_1(y - x_j), & \text{when } y < x \\ g_2(x,y) = \left(C_1 - \frac{1}{\nu}\right)(y - x_{j+1}), & \text{when } y \geq x. \end{cases} \tag{A3}$$

The final condition to obtain $C_1$ is based on the required continuity of $G(x,y)$. A discontinuous Green's function would not satisfy (A1). Therefore, we have

$$g_2(x,x) = g_1(x,x) = C_1(x - x_j) = (C_1 - \nu^{-1})(x - x_{j+1}) \tag{A4}$$

$$\Rightarrow\ C_1 = -\frac{1}{\nu}\frac{x - x_{j+1}}{x_{j+1} - x_j}. \tag{A5}$$

After simplification, we obtain the following Green's function for the diffusion operator:

$$G(x,y) = \begin{cases} g_1(x,y) = -\frac{1}{\nu}\left(\frac{x - x_{j+1}}{x_{j+1} - x_j}\right)(y - x_j), & \text{when } y < x \\ g_2(x,y) = -\frac{1}{\nu}\left(\frac{x - x_j}{x_{j+1} - x_j}\right)(y - x_{j+1}), & \text{when } y \geq x. \end{cases} \tag{A6}$$

We obtain the averaged quantity $\tau$ from definition (32). Note that the domains of integration, and averaging, become the element spatial domain. We translate the domain of the PDE to the origin, replacing $x_j$ and $x_{j+1}$ with 0 and $h$. This significantly simplifies integration.

$$\begin{aligned}
\tau &= \frac{1}{h}\int_0^h\int_0^h G(x,y)\,\mathrm{d}x\mathrm{d}y = \frac{1}{h}\int_0^h\int_0^x g_1(x,y)\,\mathrm{d}y\mathrm{d}x + \frac{1}{h}\int_0^h\int_x^h g_2(x,y)\,\mathrm{d}y\mathrm{d}x \\
&= -\frac{1}{h\nu}\int_0^h\int_0^x \left(\frac{x}{h}-1\right) y\mathrm{d}y\mathrm{d}x - \frac{1}{h\nu}\int_0^h\int_x^h \frac{x}{h}(y-h)\,\mathrm{d}y\mathrm{d}x \\
&= -\frac{1}{h\nu}\int_0^h \left(\frac{x}{h}-1\right)\frac{1}{2}x^2\,\mathrm{d}x - \frac{1}{h\nu}\int_0^h \frac{x}{h}\left(-\frac{1}{2}x^2 - \frac{1}{2}h^2 + hx\right)\mathrm{d}x \\
&= -\frac{1}{h\nu}\int_0^h \left(\frac{x^2}{2} - \frac{xh}{2}\right)\mathrm{d}x = -\frac{1}{h\nu}\left(\frac{h^3}{6} - \frac{h^3}{4}\right) = \frac{h^2}{12\nu}
\end{aligned} \tag{A7}$$

We obtain the $\gamma$ values from (32). On a one-dimensional domain, the integrals over $\partial K$ are point values at $y = 0$ and $y = h$, such that the two associated values for $\gamma$ become

$$\begin{aligned}
\gamma_0 &= \frac{1}{h}\int_0^h \frac{\mathrm{d}}{\mathrm{d}y}G(x,y)\Big|_{y=0}\,\mathrm{d}x = \frac{1}{h}\int_0^h \frac{\mathrm{d}}{\mathrm{d}y}g_1(x,y)\Big|_{y=0}\,\mathrm{d}x = -\frac{1}{\nu h}\int_0^h \left(\frac{x}{h}-1\right)\mathrm{d}x = \frac{1}{2\nu} \\
\gamma_1 &= \frac{1}{h}\int_0^h \frac{\mathrm{d}}{\mathrm{d}y}G(x,y)\Big|_{y=h}\,\mathrm{d}x = \frac{1}{h}\int_0^h \frac{\mathrm{d}}{\mathrm{d}y}g_2(x,y)\Big|_{y=h}\,\mathrm{d}x = \quad -\frac{1}{\nu h}\int_0^h \frac{x}{h}\,\mathrm{d}x = -\frac{1}{2\nu}.
\end{aligned} \tag{A8}$$

## A.2 | Reaction operator

$$\mathcal{L} = s \qquad \mathcal{L}^* = s$$

The second contribution to the fine-scale problem of the Burgers equation is the reactive component. This component does not include any differential operators, but a corresponding $\tau$ may still be computed. First, we write the Green's problem as

$$\begin{cases} sG(x,y) = \delta_x, & \text{for } y \in (x_j, x_{j+1}) \\ G(x,y) = 0, & \text{for } y \in \{x_j, x_{j+1}\}, \end{cases} \tag{A9}$$

which has the following simple solution:

$$G(x,y) = \frac{1}{s}\delta_x. \tag{A10}$$

Then, $\tau$ is obtained by double integration as

$$\tau = \frac{1}{h}\int_0^h\int_0^h \frac{1}{s}\delta_x = \frac{1}{h}\int_0^h \frac{1}{s} = \frac{1}{s}. \tag{A11}$$

Since $G(x,y)$ is independent of $y$, and thereby $g_y(x,y) = 0$, it follows that

$$\gamma_0 = 0 \tag{A12}$$

$$\gamma_1 = 0. \tag{A13}$$

## A.3 | Advection operator

$$\mathcal{L} = a \cdot \nabla \qquad \mathcal{L}^* = -a \cdot \nabla$$

The final component of the fine-scale problem of the Burgers equation is an advection operator. Note that a pure advection problem on a one-dimensional domain only has a single boundary condition; thus, the Green's problem has to be written as

$$\begin{cases} -a\frac{\mathrm{d}}{\mathrm{d}y}G(x,y) = \delta_x, & \text{for } y \in (x_j, x_{j+1}) \\ g(x,x_j) = 0 \quad \text{or} \quad g(x,x_{j+1}) = 0. \end{cases} \tag{A14}$$

Integration of the first line in this set of equations yields the Green's function

$$G(x,y) = \begin{cases} C_1, & \text{when } y < x \\ C_1 - \frac{1}{a}, & \text{when } y \geq x. \end{cases} \tag{A15}$$

We choose the boundary condition (A14) to be satisfied on the right side, such that $C_1 = 1/a$ and

$$G(x,y) = \begin{cases} \frac{1}{a}, & \text{when } y < x \\ 0, & \text{when } y \geq x. \end{cases} \tag{A16}$$

We finally obtain $\tau$ as

$$\tau = \frac{1}{h}\int_0^h \int_0^x \frac{1}{a}\mathrm{d}y\,\mathrm{d}x = \frac{1}{h}\int_0^h \frac{x}{a}\mathrm{d}x = \frac{h}{2a}. \tag{A17}$$

The temporal differential operator $\frac{\mathrm{d}}{\mathrm{d}t}$ can be viewed as an advective operator with advection speed 1. The expression for $\tau$ changes slightly. The weak formulation used in Section 4.3 makes use of a one-dimensional finite element mesh in space and a finite difference scheme in time. Since $\tau$ is an *element* average, the factor $\frac{1}{|K|}$ is $\frac{1}{h}$. However, the $x$-coordinate in the Green's function runs from $t^n$ to $t^{n+1}$ or, when translated, from 0 to $\Delta t$, which is the domain of integration. We therefore obtain

$$\tau = \frac{1}{h}\int_0^{\Delta t} \int_0^x 1 = \frac{1}{h}\int_0^{\Delta t} x = \frac{\Delta t^2}{2h}. \tag{A18}$$

Since this Green's function is piecewise constant, the derivative with respect to $y$ is zero. Therefore, the integrals in the expression for $\gamma$ vanish, and we find

$$\gamma_0 = 0 \tag{A19}$$

$$\gamma_1 = 0. \tag{A20}$$